BIOCHEMISTRY

A nucleotidyltransferase toxin inhibits growth of *Mycobacterium tuberculosis* through inactivation of tRNA acceptor stems

Yiming Cai[1]*, Ben Usher[2]*, Claude Gutierrez[3], Anastasia Tolcan[4], Moise Mansour[1], Peter C. Fineran[5,6,7], Ciarán Condon[4], Olivier Neyrolles[3], Pierre Genevaux[1†‡], Tim R. Blower[2†‡]

Toxin-antitoxin systems are widespread stress-responsive elements, many of whose functions remain largely unknown. Here, we characterize the four DUF1814-family nucleotidyltransferase-like toxins ($MenT_{1–4}$) encoded by the human pathogen *Mycobacterium tuberculosis*. Toxin $MenT_3$ inhibited growth of *M. tuberculosis* when not antagonized by its cognate antitoxin, $MenA_3$. We solved the structures of toxins $MenT_3$ and $MenT_4$ to 1.6 and 1.2 Å resolution, respectively, and identified the biochemical activity and target of $MenT_3$. $MenT_3$ blocked in vitro protein expression and prevented tRNA charging in vivo. $MenT_3$ added pyrimidines (C or U) to the 3′-CCA acceptor stems of uncharged tRNAs and exhibited strong substrate specificity in vitro, preferentially targeting $tRNA^{Ser}$ from among the 45 *M. tuberculosis* tRNAs. Our study identifies a previously unknown mechanism that expands the range of enzymatic activities used by bacterial toxins, uncovering a new way to block protein synthesis and potentially treat tuberculosis and other infections.

INTRODUCTION

Toxin-antitoxin (TA) systems are widely distributed throughout prokaryotic genomes and have been shown to help bacteria to survive predation by bacteriophages, immune responses, and antibiotic treatments (*1*–*5*). In many cases, however, the roles of chromosomal TA systems remain largely unknown, primarily due to the lack of a phenotype associated with deletion mutants under in vitro laboratory conditions (*6*–*9*). TA systems are also widespread among mobile genetic elements, including plasmids, superintegrons, cryptic prophages, and conjugative transposons, where they contribute to their stability (*10*, *11*).

TA systems encode two components, a toxic protein that targets an essential cellular process and an antagonistic antitoxin, which blocks toxin activity when cells are growing under favorable conditions. Although the processes that lead to toxin activation remain under debate, it has been proposed that under certain stress conditions, increased toxin transcription and synthesis may lead to activation (*8*, *12*). This, in turn, reduces growth rate, which can provide a means to survive with minimal metabolic burden until favorable conditions return (*13*).

TA systems are divided into six types according to the nature of the toxin and antitoxin (whether they are RNA or protein) and the mechanism of toxin antagonism (*3*). Type II systems, in which a protein toxin is sequestered by a protein antitoxin, have been most extensively studied. They are also remarkably abundant in *Mycobacterium tuberculosis*, which potentially encodes more than 80 type II TA systems, and are thought to have contributed to the success of *M. tuberculosis* as a human pathogen (*14*–*16*). Many of the putative *M. tuberculosis* toxins tested thus far were shown to inhibit bacterial growth, suggesting that these TA systems are functionally active and could modulate *M. tuberculosis* growth under certain conditions, thereby contributing to survival in the human host (*15*, *17*). Accordingly, many *M. tuberculosis* TA operons were shown to be induced in response to relevant stressors, including hypoxia, the presence of antimicrobial drugs, or macrophage engulfment (*14*, *17*). As *M. tuberculosis* encodes, among others, more than 50 VapBC, 10 MazEF, 3 HigBA, and 3 RelBE TA systems, it might be expected that there is redundancy between them, alongside condition-specific applications for each system. Furthermore, the highly toxic nature of some of these toxins suggests that their antibacterial mechanisms could be developed into antimicrobials (*18*).

This study focuses on a family of four putative toxins from *M. tuberculosis*, namely, Rv0078A, Rv0836c, Rv1045, and Rv2826c, which share a conserved nucleotidyltransferase (NTase)–like domain annotated as domain of unknown function (DUF) 1814 (Fig. 1A). The most well-characterized example of this DUF1814 family is AbiEii from *Streptococcus agalactiae*, which shares 18.3% sequence identity with Rv1045, and was identified within the AbiE abortive infection bacteriophage-defense systems (*19*). AbiEii was shown to constitute a new type of TA system, type IV, based on the observation that no interaction could be detected between the toxin and the antitoxin proteins (*20*). The DUF1814 family of proteins is widespread in bacterial, archaeal, and fungal genomes (*20*), though not all examples are genetically linked to putative antitoxins. As putative NTases, DUF1814 proteins contain four conserved motifs. The N-terminal motifs I and II are found in DNA polymerase β and are proposed to coordinate a metal ion for nucleotide binding and

[1]Laboratoire de Microbiologie et Génétique Moléculaires, Centre de Biologie Intégrative, Université de Toulouse, CNRS, UPS, 118 route de Narbonne, 31400 Toulouse, France. [2]Department of Biosciences, Durham University, South Road, Durham DH1 3LE, UK. [3]Institut de Pharmacologie et de Biologie Structurale, IPBS, Université de Toulouse, CNRS, UPS, 205 route de Narbonne, 31400 Toulouse, France. [4]UMR8261 (CNRS, Université de Paris), Institut de Biologie Physico-Chimique, 13 rue Pierre et Marie Curie, 75005 Paris, France. [5]Department of Microbiology and Immunology, University of Otago, PO Box 56, Dunedin 9054, New Zealand. [6]Genetics Otago, University of Otago, PO Box 56, Dunedin 9054, New Zealand. [7]Bio-protection Research Centre, University of Otago, PO Box 56, Dunedin 9054, New Zealand.
*These authors contributed equally to this work.
†Co–senior authors.
‡Corresponding author. Email: genevaux@ibcg.biotoul.fr (P.G.), timothy.blower@durham.ac.uk (T.R.B.)

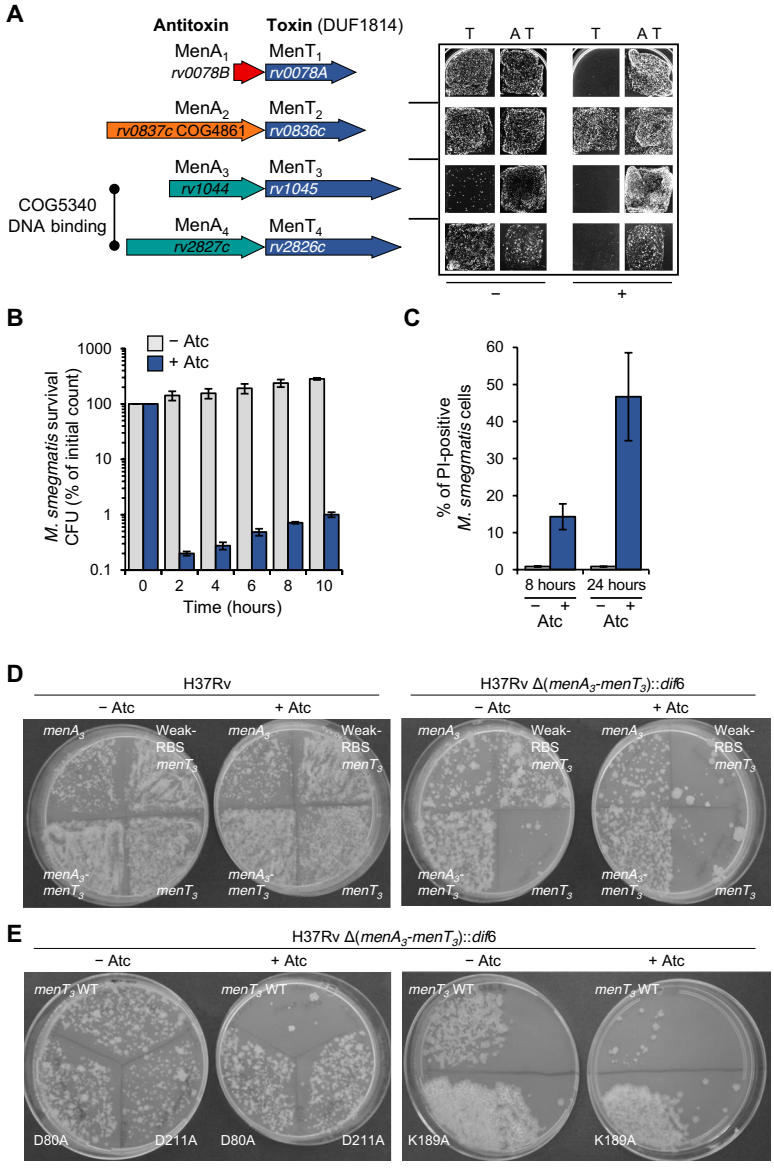

Fig. 1. Analysis of the four TA systems with NTase-like toxins encoded by the *M. tuberculosis* genome. (**A**) Scaled representation of the four *M. tuberculosis* TA systems containing NTase-like toxin genes with original and revised nomenclature (left), and corresponding toxicity and antitoxicity assays in *M. smegmatis* (right). For toxicity and antitoxicity assays, cotransformants of *M. smegmatis* mc^2 155 containing pGMC-vector, -$MenT_1$, -$MenT_2$, -$MenT_3$, or -$MenT_4$ (toxins) and pLAM-vector, -$MenA_1$, -$MenA_2$, -$MenA_3$, or -$MenA_4$ (antitoxins) were plated on LB-agar in the presence or absence of anhydrotetracycline (Atc; 100 ng ml^{-1}) and acetamide (Ace; 0.2%) inducers for toxin and antitoxin expression, respectively. Plates were incubated for 3 days at 37°C. "T" and "A" denote toxin and antitoxin, respectively. "–" and "+" represent absence or presence of inducer, respectively. (**B**) *M. smegmatis* strain mc^2 155 transformed with plasmid pGMCS-TetR-P1-RBS1-$MenT_3$ was grown in complete 7H9 medium with Sm. At time 0, the culture was divided into two. Half was kept in the same medium (pale blue bars) and half was additionally treated with Atc (200 ng ml^{-1}) (dark blue bars). Samples were harvested at the indicated times, washed, diluted, and plated on LB-agar with Sm but without Atc. Colonies were counted after 3 days at 37°C. Shown values are the average of three biological replicates with SD. CFU, colony-forming unit. (**C**) Samples of the same cultures as in (B) were harvested after 8 or 24 hours, labeled with the LIVE/DEAD BacLite dyes [Syto 9; propidium iodide (PI)], and analyzed by fluorescence-activated cell sorting. The percentage of PI-positive cells is shown for each sample (pale blue bars, no Atc; dark blue bars, 200 ng ml^{-1} Atc). Shown values are the average of three biological replicates with SD. (**D**) *M. tuberculosis* wild-type (WT) H37Rv or mutant strain H37Rv Δ(*$menA_3$-$menT_3$*)::*dif*6 were transformed with 100 ng of plasmids expressing either *$menA_3$*, *$menT_3$*, or *$menA_3$-$menT_3$*. These plasmids encode a consensus Shine-Dalgarno sequence (RBS1), except for "Weak-RBS-*$menT_3$*," which encodes a near-consensus sequence (RBS4) to weaken expression. After phenotypic expression, half of the transformation mix was plated on 7H11 oleic acid–albumin-dextrose-catalase (OADC) plates with Sm, and the other half was plated on 7H11 OADC Sm plates supplemented with Atc (200 ng ml^{-1}). Plates were imaged after 20 days at 37°C; data are representative of three independent experiments. (**E**) Mutant strain H37Rv Δ(*$menA_3$-$menT_3$*)::*dif*6 was transformed with 100 ng of plasmids expressing either *$menT_3$* WT or mutant alleles introducing the D80A, K189A, or D211A substitutions. After phenotypic expression, half of the transformation mix was plated on 7H11 OADC plates with Sm, and the other half was plated on 7H11 OADC Sm plates supplemented with Atc (200 ng ml^{-1}). Pictures were taken after 20 days at 37°C; data are representative of three independent experiments.

transfer (*20*). The C-terminal motif III is similar to that of tRNA NTases that add the 3′-CCA motif to immature tRNAs and may be important for base stacking with substrates (*21*). The C-terminal motif IV is unique to DUF1814 proteins and is proposed to form a catalytic site with motif III (*20*).

In *M. tuberculosis*, the DUF1814 toxins are encoded downstream of a variety of putative antitoxins (Fig. 1A). The toxin gene *rv0078A* is paired with a short upstream open reading frame encoding a 68–amino acid antitoxin, Rv0078B, related to MazE antitoxins, which is predicted to be disordered and lacking a DNA-binding domain (*16*). Toxin gene *rv0836c* lies downstream of a COG4861 gene, encoding a much larger putative antitoxin than the cognate toxin (Fig. 1A). Rv1045 and Rv2826c toxins are downstream of their cognate putative antitoxins Rv1044 and Rv2827c, respectively, both of which are COG5340 transcriptional regulator family proteins (Fig. 1A). COG5340 proteins include the *S. agalactiae* AbiEi antitoxin partner of AbiEii, which has previously been shown to bind to and repress the *abiE* promoter, similar to autoregulation observed in type II TA loci (*22*). An earlier transposon site hybridization study identified both the Rv1044 and Rv2827c antitoxins as essential for growth (*23*). Saturating transposon mutagenesis has additionally demonstrated that Rv1044 is essential, while transposon insertions in Rv2827c impart a growth defect (*24*). The fact that both antitoxins are important for *M. tuberculosis* growth strongly suggests that their putative cognate Rv1045 and Rv2826c toxins inhibit growth in *M. tuberculosis*.

Here, we undertook a series of microbiological, structural, genetic, and biochemical studies to investigate the DUF1814 toxins of *M. tuberculosis* and reveal their mode of action. We show that the Rv1045 toxin is a tRNA NTase that is active in *M. tuberculosis* and blocks translation through a previously undescribed mechanism involving inactivation of serine tRNAs.

RESULTS

Three DUF1814 proteins are part of bona fide TA systems

We first investigated the activity of the putative TA systems containing NTase-like DUF1814 toxins in *Mycobacterium smegmatis*, which is closely related to *M. tuberculosis* and does not encode similar antitoxins (*15*). On the basis of the findings presented below, we renamed these putative systems as "mycobacterial AbiE-like NTase toxins" (MenT) and antitoxins (MenA), numbered according to their order in the *M. tuberculosis* genome (Fig. 1A). Toxins and antitoxins were expressed in trans, with the toxins cloned into the pGMC-integrative plasmid under the control of an anhydrotetracycline (Atc)–inducible promoter and the antitoxins into the compatible pLAM plasmid under the control of an acetamide (Ace)–inducible promoter (Fig. 1A). Among the four putative toxins, only $MenT_1$ has been tested so far and was shown to be toxic in *M. smegmatis* when expressed without the upstream open reading frame encoding $MenA_1$, suggesting that $MenA_1$-$MenT_1$ form a functional TA system (*16*). Accordingly, the data presented in Fig. 1A show that $MenT_1$ toxicity was efficiently counteracted by $MenA_1$ expressed in trans. Both $MenA_3$-$MenT_3$ and $MenA_4$-$MenT_4$ also acted as TA pairs, while $MenT_2$ expression was not toxic (Fig. 1A). Inhibition of $MenT_4$ toxicity could only be achieved when the putative antitoxin was expressed in the context of the *menA*$_4$-*menT*$_4$ operon (Fig. 1A). Expression of $MenA_4$ alone from pLAM was toxic (fig. S1A), indicating that $MenA_4$-$MenT_4$ might not function as a typical TA pair under these conditions. Similar experiments performed in *Escherichia coli* confirmed the phenotypes observed in *M. smegmatis* for $MenA_2$-$MenT_2$, $MenA_3$-$MenT_3$, and $MenA_4$-$MenT_4$ (including $MenA_4$ toxicity), but not for $MenT_1$, which exhibited no detectable toxicity in *E. coli* (fig. S1B). Last, coexpression of the active toxins with noncognate antitoxins did not reveal any detectable cross-talk between the different TA pairs (fig. S1, A and C). Note that cross-talk assays with $MenA_4$ antitoxin expressed from pLAM in *M. smegmatis* could not be performed because of its toxicity.

Ectopic expression of $MenT_3$ in the presence of inducer showed the most robust toxicity in both *M. smegmatis* and *E. coli* when compared to the other toxins (Fig. 1A and fig. S1). In *M. smegmatis*, only a few $MenT_3$ transformants were obtained, even in the absence of inducer. Ectopic expression of $MenT_3$ in *M. smegmatis* induced a rapid drop of about 3-$\log_{10}$ in colony-forming units only 2 hours after induction with Atc (Fig. 1B). LIVE/DEAD BacLight stains have previously been used to study the effects of toxin expression on cell viability in *M. tuberculosis* (*18*). Flow cytometry analysis of *M. smegmatis* expressing $MenT_3$ revealed that the proportion of propidium iodide–permeable cells was substantially higher in $MenT_3$-induced versus noninduced cells 8 or 24 hours after induction with Atc (Fig. 1C), indicating that $MenT_3$ strongly affects cell viability.

$MenA_3$-$MenT_3$ is a functional TA system in *M. tuberculosis*

To investigate the impact of $MenA_3$ and $MenT_3$ on *M. tuberculosis* growth, plasmids encoding the toxin, the antitoxin, or both, were introduced into H37Rv wild-type (WT) strain. The resulting transformants were not sensitive to ectopic expression of $MenT_3$ (Fig. 1D), presumably because endogenous $MenA_3$ was sufficient to neutralize the sum of endogenous and ectopic $MenT_3$. To confirm this hypothesis, we attempted to construct a strain deleted for the *menA*$_3$-*menT*$_3$ operon. Previous work showed that *menA*$_3$ cannot be disrupted by transposon insertion (*24*). Accordingly, we found that deletion of the *menA*$_3$-*menT*$_3$ operon in *M. tuberculosis* H37Rv strain could not be achieved, most likely because simultaneous disruption of both genes resulted in a toxic effect from residual $MenT_3$. To circumvent this problem, we constructed the deletion in a derivative of H37Rv carrying a second copy of *menA*$_3$ constitutively expressed from a pGMC integrative plasmid. Once the *menA*$_3$-*menT*$_3$ operon was deleted, it was then possible to remove the ectopic copy of *menA*$_3$ by pGMC plasmid replacement (fig. S2). The Δ*menA*$_3$-*menT*$_3$ mutant became highly sensitive to the $MenT_3$ toxin, even in the absence of inducer (Fig. 1D). Therefore, to finally obtain transformants, *menT*$_3$ was cloned downstream of a weaker Shine-Dalgarno sequence. Using this construct, we observed inducible $MenT_3$ toxicity, which was fully abolished by the presence of the antitoxin (Fig. 1D). Together, these data demonstrate that the $MenT_3$ toxin inhibits growth and that $MenA_3$-$MenT_3$ functions as a bona fide TA pair in *M. tuberculosis*.

A previous amino acid sequence alignment of DUF1814 putative NTases highlighted conserved residues, a number of which were confirmed as essential for AbiEii toxicity in *S. agalactiae* (*20*). To investigate whether some of these residues were important for $MenT_3$ toxicity, we selected and engineered three conserved residues for substitution: D80A, localized in the DNA polβ superfamily motif, and K189A and D211A, both toxin-specific residues. We then tested the impact of these substitutions on *M. tuberculosis* growth (Fig. 1E). All three substitutions abolished $MenT_3$ toxicity in both *M. tuberculosis* (Fig. 1E) and *E. coli* (fig. S3A).

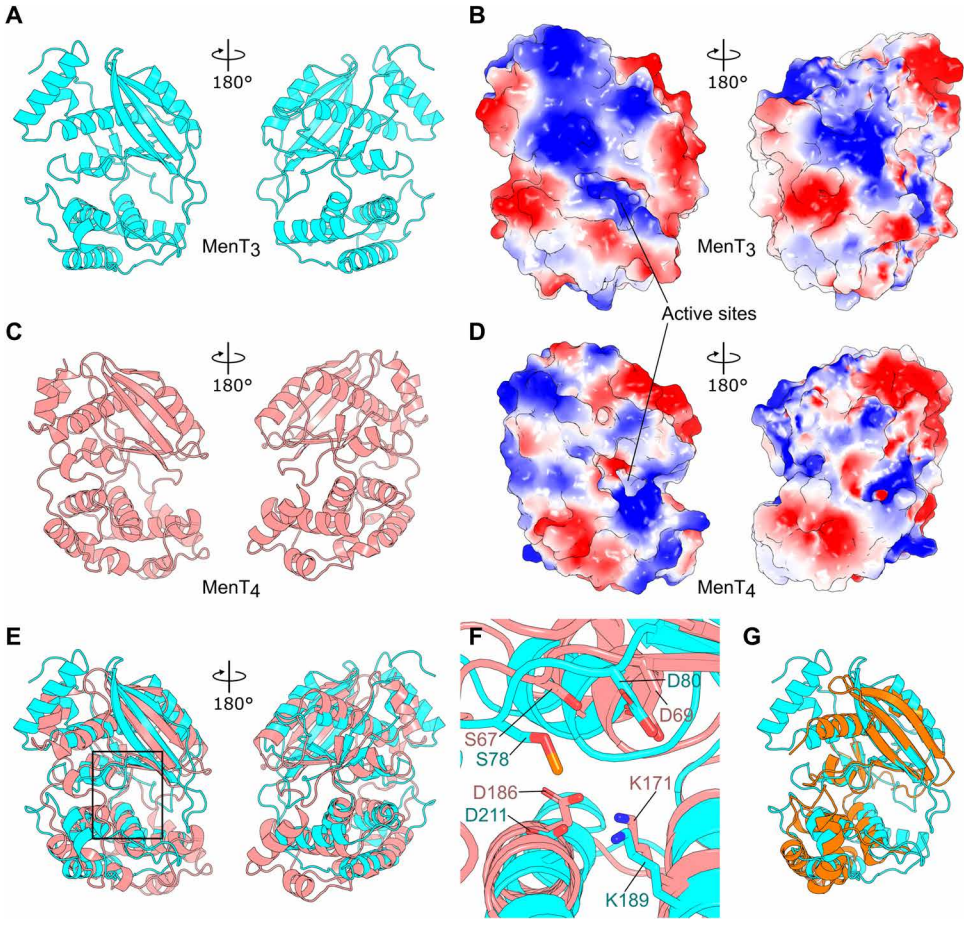

Fig. 2. Crystal structure of the $MenT_3$ and $MenT_4$ toxins. (**A**) Structure of monomeric $MenT_3$ toxin, with views from front and back, shown as cyan cartoon representations. (**B**) Surface electrostatics of $MenT_3$, viewed as in (A), with red for electronegative and blue for electropositive potential. (**C**) Structure of monomeric $MenT_4$, with views from front and back, shown as salmon cartoon representations. (**D**) Surface electrostatics of $MenT_4$, viewed as in (C), colored as per (B). (**E**) Superposition of $MenT_4$ onto $MenT_3$, viewed and colored as per (A) and (C). (**F**) Tilted close-up view of the toxin active sites, as indicated by the boxed region of (E). $MenT_3$ residues S78 (phosphorylated), D80, K189, and D211 are indicated, along with the homologous $MenT_4$ residues S67, D69, K171, and D186. (**G**) Alignment of JHP933 (PDB: 4O8S) as orange cartoon representation, against $MenT_3$ viewed and colored as per (A, left).

Next, we investigated whether the $MenT_3$ toxin and $MenA_3$ antitoxin could interact in vivo. Since this TA pair is functional in *E. coli*, we performed affinity-tagged in vivo copurification experiments in *E. coli* using His-tagged variants of $MenT_3$ and $MenA_3$, which were first confirmed to be active as toxin and antitoxin, respectively (fig. S4A). In strains coexpressing both the toxin and the antitoxin (with either the toxin or the antitoxin tagged), and with tagged toxin and tagged antitoxin alone as controls, the in vivo copurification revealed that a small but significant fraction of the $MenT_3$ toxin and the $MenA_3$ antitoxin copurified, whether the toxin or the antitoxin was used as bait (fig. S4, C and D). Similar results were obtained with the $MenA_1$-$MenT_1$ pair, which encodes a much shorter, unrelated antitoxin (fig. S4, B, E, and F). Together, these data show that both TA partners can interact, but it remains to be determined whether a direct interaction between an NTase toxin and its cognate antitoxin is required for toxin inhibition.

$MenT_3$ and $MenT_4$ are structural homologs

To begin investigations into the mechanism of toxicity of $MenT_3$, we solved its structure to 1.6 Å resolution by x-ray crystallography (Fig. 2A and Table 1). $MenT_3$ is a monomeric bi-lobed globular protein, with two hemispheres connected by a short linker (Fig. 2A). This monomeric assembly matches the expected size observed by size exclusion chromatography. Surface electrostatics show a distinct electropositive surface leading to a deeper recess (Fig. 2B, left), which contains residues D80, K189, and D211 that were needed for toxicity in vivo (Fig. 1E). This potentially indicates the position of the active site, and the electropositive surface may facilitate interaction with electronegative substrates such as nucleic acids. To further characterize the DUF1814 family, we also solved the $MenT_4$ toxin structure to 1.2 Å resolution (Fig. 2C and Table 1). $MenT_4$ is also monomeric (also observed by size exclusion chromatography) and the overall architecture is similar to, but not exactly the same as, $MenT_3$. $MenT_4$ has a bi-lobed globular structure and distinct electropositive patches close to a similarly positioned active site region (Fig. 2, C and D). Aligning $MenT_3$ and $MenT_4$ by sequence gave a poor root mean square deviation (RMSD) of 13.4 Å; however, this can be improved to 4.7 Å using sequence-independent superposition, which demonstrates similarity in overall fold (Fig. 2E). A close-up of $MenT_3$ residues D80, K189, and D211 show them

Table 1. Crystallographic data collection and refinement statistics.

	$MenT_3$ native	$MenT_3$ Se-peak	$MenT_3$ Se-high remote	$MenT_3$ Se-inflection	$MenT_4$ native
Data collection					
PDB ID code	6Y5U	-	-	-	6Y56
Beamline	Diamond I04	Diamond I03	Diamond I03	Diamond I03	Diamond I24
Wavelength (Å)	0.9795	0.9793	0.9641	0.9795	0.9781
Resolution range (Å)	47.70–1.59 (1.65–1.59)*	47.78–2.19 (2.26–2.19)	47.83–2.05 (2.11–2.05)	53.13–2.04 (2.11–2.04)	42.23–1.23 (1.27–1.23)
Space group	$P3_221$	$P3_221$	$P3_221$	$P3_221$	$P2_1$
Unit cell, *a b c* (Å), α β γ (°)	95.4 95.4 69.0, 90.0 90.0 120.0	95.6 95.6 69.2, 90.0 90.0 120.0	95.7 95.7 69.3, 90.0 90.0 120.0	95.6 95.6 69.3, 90.0 90.0 120.0	42.3 57.8 54.7, 90.0 92.3 90.0
Total reflections	98,016 (9668)	36,407 (3179)	44,514 (3476)	47,255 (4637)	149,653
Unique reflections	49,008 (4834)	19,130 (1646)	23,313 (1788)	23,628 (2319)	75,996 (7206)
Multiplicity	2.0	1.9	1.9	2.0	2.0
Completeness (%)	99.95 (99.83)	100.00 (100.00)	100.00 (99.80)	100.00 (99.70)	98.80 (88.97)
Mean $I/\sigma(I)$	16.7	6.5	7.6	8.9	7.0
R_{merge}	0.016 (0.486)	0.055 (0.373)	0.055 (0.522)	0.048 (0.463)	0.060 (0.926)
R_{meas}	0.022 (0.687)	0.077 (0.528)	0.078 (0.739)	0.068 (0.654)	0.085 (1.310)
$CC_{1/2}$	1.0 (0.672)	0.995 (0.803)	0.997 (0.544)	0.997 (0.641)	0.996 (0.294)
Refinement					
R_{work}	0.2024 (0.2924)	-	-	-	0.1840 (0.3174)
R_{free}	0.2242 (0.3108)	-	-	-	0.1950 (0.3352)
No. of non-hydrogen atoms	2494	-	-	-	2649
Macromolecules	2213	-	-	-	2322
Solvent	281	-	-	-	327
Protein residues	288	-	-	-	292
RMSD (bonds, Å)	0.006	-	-	-	0.005
RMSD (angles, °)	0.940	-	-	-	0.830
Ramachandran favored (%)	97.53	-	-	-	98.28
Ramachandran allowed (%)	2.47	-	-	-	1.72
Ramachandran outliers (%)	0.00	-	-	-	0.00
Average *B* factor	34.1	-	-	-	20.6
Macromolecules	33.4	-	-	-	19.3
Solvent	39.4	-	-	-	29.9

*Statistics for the highest-resolution shell are shown in parentheses.

clustered at the putative active site, and when overlaid, the homologous $MenT_4$ residues, D69, K171, and D186, respectively, take up similar positions (Fig. 2F). There was also density for a phosphoserine at $MenT_3$ S78, but the corresponding residue in $MenT_4$, S67, was not phosphorylated (Fig. 2F). Searches for structural homologs of $MenT_3$ and $MenT_4$ were performed using the DALI server (*25*). Among multiple hits for NTases, the best match was for JHP933 from *Helicobacter pylori*, a predicted NTase encoded by the *jhp0933* gene (*26*). JHP933 aligned to $MenT_3$ with an RMSD of 2.4 Å, though multiple additional helices were resolved in the $MenT_3$ structure (Fig. 2G). An analysis of the *H. pylori* genome revealed that the *jhp0932* gene lies just upstream of *jhp0933* and partially overlaps its coding sequence. The presence of these genes in what appears to be a classic TA configuration suggests that JHP933 may belong to the $MenT_3$/$MenT_4$ family of NTase-like toxins.

RNase PH overexpression confers resistance to $MenT_3$

$MenT_3$ is the most toxic of the four *M. tuberculosis* NTase-like toxins tested, both in mycobacteria and in *E. coli* (Fig. 1 and fig. S1). We therefore took advantage of this robust toxicity to search for *E. coli* genes that were able to suppress $MenT_3$-mediated growth inhibition when overexpressed. We reasoned that identification of such

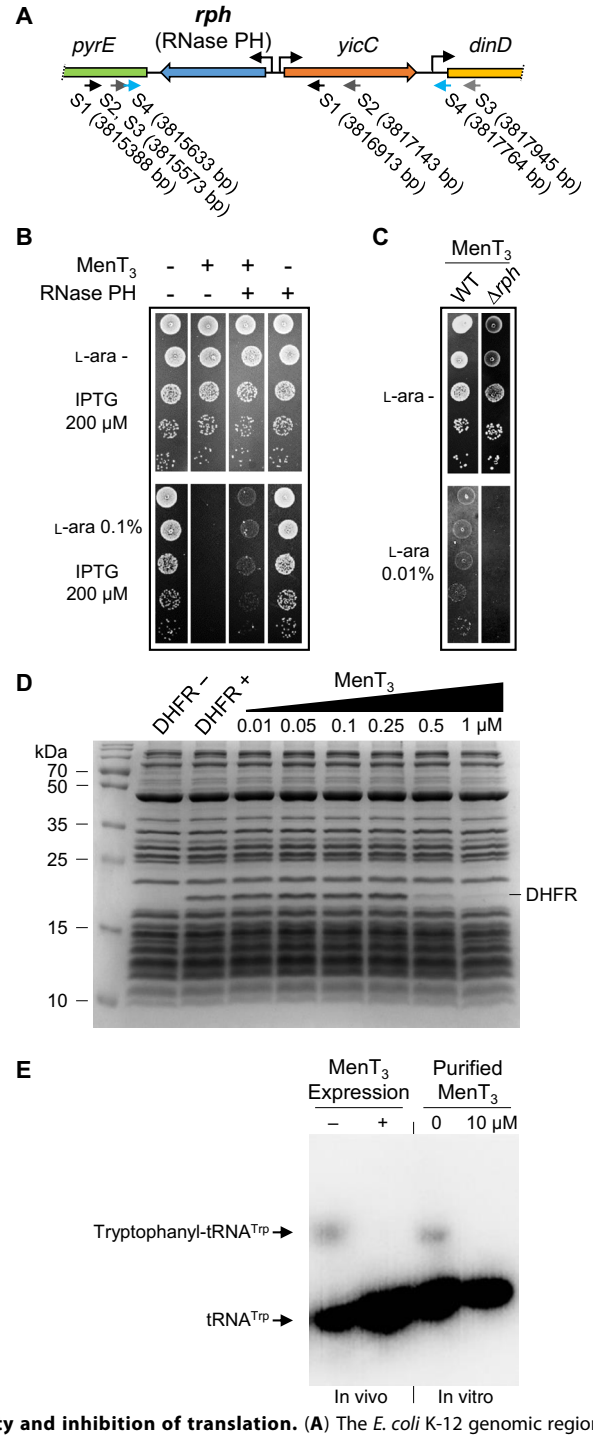

Fig. 3. RNase PH suppresses MenT$_3$ toxicity and inhibition of translation. (**A**) The *E. coli* K-12 genomic region containing the *rph* gene is shown. Suppressor plasmids that counteract MenT$_3$ toxicity encoded *rph*, as depicted by small arrows under the adjacent genes *pyrE*, *yicC*, and *dinD*. The positions in base pair of the ends of each suppressor fragment, in relation to the *E. coli* K-12 chromosome, are indicated between brackets. (**B**) Overexpression of *E. coli* RNase PH partially suppresses MenT$_3$ toxicity. *E. coli* DLT1900 strains containing either pK6-vector (–) or pK6-MenT$_3$ (+) were cotransformed with p29SEN-vector (–) or p29SEN-Rph (RNase PH) (+). The resulting cotransformants were serially diluted, spotted onto LB-agar plates in the presence or absence of L-ara (0.1%) and IPTG (200 µM) inducers, and incubated at 37°C. (**C**) Deletion of *rph* further increases MenT$_3$ toxicity. Transformants of *E. coli* DLT1900 WT and Δ*rph* mutant strains containing plasmid pK6-MenT$_3$ were serially diluted, spotted onto LB-agar plates with or without L-ara (0.01%), and incubated at 37°C. (**D**) In vitro transcription/translation reactions assessing levels of DHFR control protein produced in the absence or presence of increasing concentrations of MenT$_3$ toxin. Samples were separated by SDS–polyacrylamide gel electrophoresis and stained with InstantBlue. (**E**) For in vivo assays, transformants of *E. coli* BL21 (λDE3) containing plasmid pET-MenT$_3$ or the empty vector were grown in M9M at 37°C. Following overexpression of MenT$_3$, tRNAs were extracted, separated, and visualized by Northern blot using specific radiolabeled probes against tRNA^{Trp}. For in vitro assays, purified MenT$_3$ (10 µM) was added to transcription/translation assays producing GatZ protein. After 2 hours at 37°C, tRNAs were extracted, separated, and visualized by Northern blot as performed for the in vivo samples. All images are representative of triplicate data.

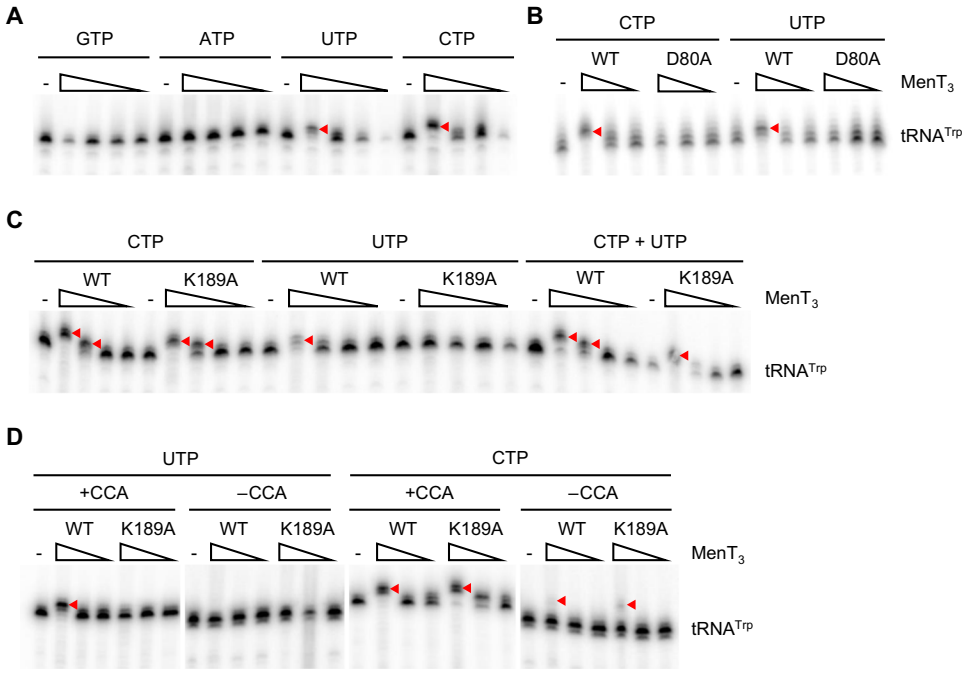

Fig. 4. Toxin $MenT_3$ adds pyrimidines to the 3′-CCA acceptor stem of tRNA. (**A**) Radiolabeled *E. coli* $tRNA^{Trp}$ was incubated with 1, 0.1, 0.01, or 0.001 μg of $MenT_3$ WT or no toxin (–) for 20 min at 37°C in the presence of unlabeled GTP, ATP, UTP, or CTP. Extended products are indicated with arrowheads throughout all panels. (**B**) Radiolabeled *E. coli* $tRNA^{Trp}$ was incubated with 1, 0.1, or 0.01 μg of $MenT_3$ WT or $MenT_3^{(D80A)}$ with CTP or UTP, as per conditions in (A). (**C**) Incubation of radiolabeled *E. coli* $tRNA^{Trp}$ with 1, 0.1, 0.01, or 0.001 μg of $MenT_3$ WT or $MenT_3^{(K189A)}$, with CTP, UTP, or a mixture of both, as per conditions in (A). (**D**) Radiolabeled *E. coli* $tRNA^{Trp}$ preparations, made with or without a 3′-CCA motif, were incubated with 1, 0.1, or 0.01 μg of either $MenT_3$ WT, $MenT_3^{(K189A)}$, or no toxin (–), for 20 min at 37°C in the presence of unlabeled UTP or CTP. Note that the (–) CCA lanes have been overexposed to equalize intensity to the (+) CCA lanes of the same gel. Assays of the individual WT and $MenT_3$ substitution proteins and $tRNA^{Trp}$ ± CCA substrates shown in (A) to (D) were performed between two and four times.

suppressors might potentially shed light on the cellular processes affected by the toxin. Details of the genetic selection used are described in Materials and Methods. Among the approximately 60,000 clones of the *E. coli* genomic plasmid library tested in this work, we identified 18 plasmids that passed two rounds of selection and appeared to encode bona fide suppressors of $MenT_3$ toxicity. We observed that the toxin-resistant colonies were noticeably smaller and translucent compared to noninduced cells, indicating that, although notably reduced, $MenT_3$ toxicity is not fully suppressed. Sequencing of the genomic regions encoded by the 18 suppressor plasmids revealed that several of these candidate plasmids harbored the same genomic fragments. Six different suppressor clones encompassing two different regions of the *E. coli* chromosome were identified. Two of the six suppressor plasmids harbored the *ydeA* gene, encoding an L-arabinose (L-ara) exporter protein known to decrease L-ara levels in *E. coli* (*27*). These suppressors were discarded as YdeA overexpression would presumably decrease toxicity of many toxic proteins expressed from the *araBAD* promoter. The four other suppressor plasmids harbored the *rph* gene, encoding the phosphorolytic ribonuclease (RNase PH), involved in the 3′ processing of RNAs (Fig. 3A). RNase PH removes nucleotides downstream of the 3′-CCA sequence, required for aminoacylation of tRNAs, from tRNA precursors with 3′ extensions. It is also involved in other RNA maturation and quality control processes, including the maturation of rRNA (*28*).

Suppression of $MenT_3$ toxicity by RNase PH overexpression was confirmed by cloning *rph* alone in a low–copy number plasmid under the control of an isopropyl-β-D-thiogalactopyranoside (IPTG)–inducible promoter and assaying for growth in the presence of $MenT_3$ in *E. coli* (Fig. 3B). We also showed that the toxicity of $MenT_3$ was enhanced when expressed in *E. coli* carrying a deletion of the *rph* gene, even with a 10-fold decrease in inducer levels (Fig. 3C), further reinforcing the genetic link between $menT_3$ and *rph*. The primary role of RNase PH in processing tRNAs suggests that DUF1814 NTase-like toxins could act directly at the site of aminoacylation at the 3′-end of tRNA, thus inhibiting translation. Whether endogenous RNase PH would be sufficiently induced in response to toxin expression to help restore the functional tRNA pool in recovering *M. tuberculosis* cells remains to be determined.

$MenT_3$ inhibits tRNA charging

$MenT_3$ WT and the $MenT_3^{(D80A)}$ and $MenT_3^{(K189A)}$ substitutions were overexpressed and purified for biochemical characterization. When tested in an in vitro transcription/translation reaction that uses recombinant *E. coli* components, purified $MenT_3$ WT reduced production of the *E. coli* dihydrofolate reductase (DHFR) control protein in a concentration-dependent manner (Fig. 3D). Compared to $MenT_3$ WT, $MenT_3^{(D80A)}$ and $MenT_3^{(K189A)}$ had a markedly reduced impact on the production of DHFR (fig. S5A). The same trend was observed when $MenT_3$ WT, $MenT_3^{(D80A)}$, and $MenT_3^{(K189A)}$ were used in in vitro reactions producing WaaF and GatZ as test proteins (fig. S5, B and C). We also expressed and purified $MenT_4$ WT and demonstrated that this, too, prevented the production of DHFR in a concentration-dependent manner in in vitro transcription/translation assays (fig. S5D).

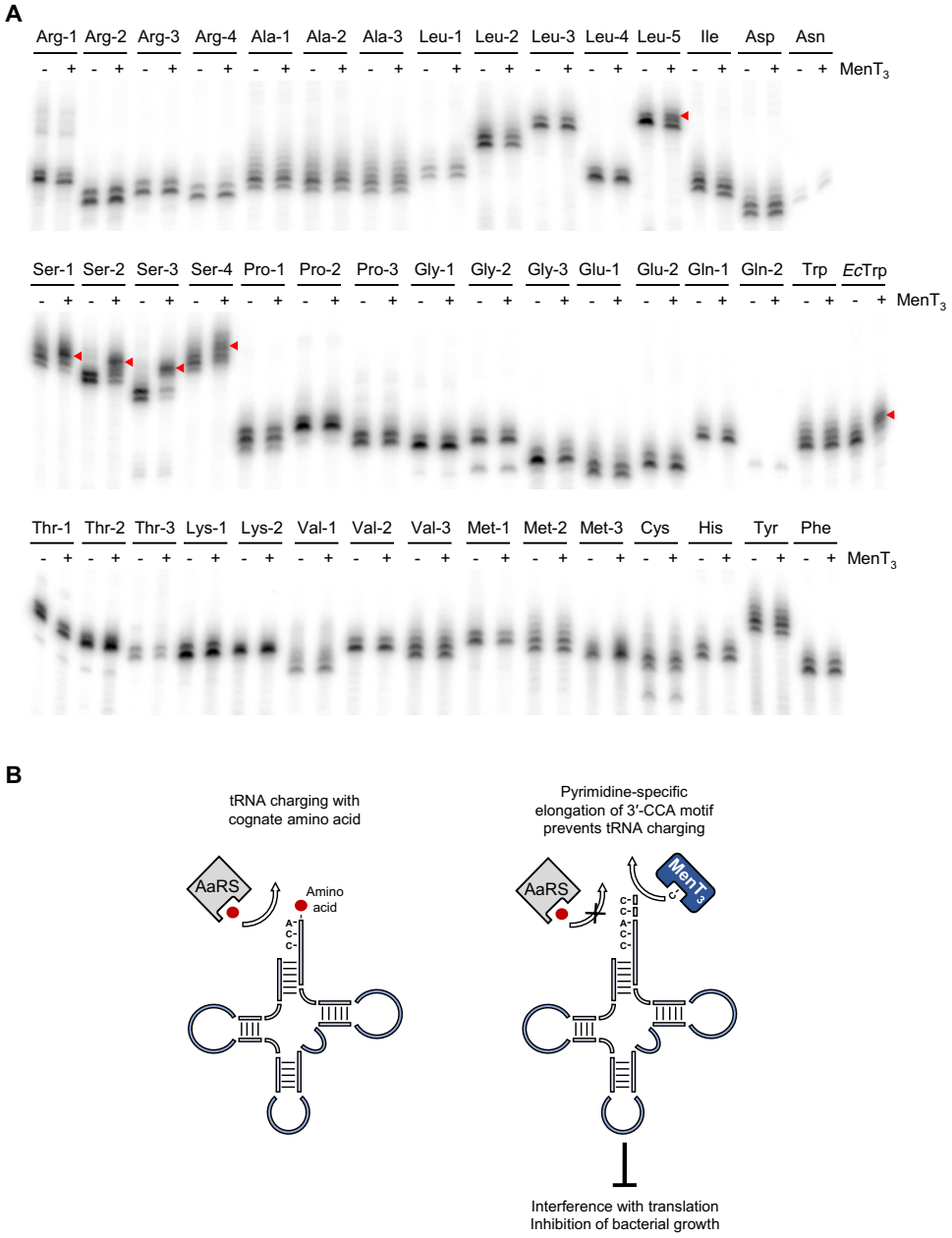

Fig. 5. Screening for $MenT_3$ *M. tuberculosis* tRNA targets. (**A**) Radiolabeled *M. tuberculosis* tRNAs were incubated with 0.1 μg of $MenT_3$ WT (+) or no toxin (–) for 20 min at 37°C in the presence of unlabeled CTP. *E. coli* $tRNA^{Trp}$ (EcTrp) was used as a positive control. The global screen of all *M. tuberculosis* tRNA was performed once and the effect of $MenT_3$ $tRNA^{Ser2}$ was confirmed twice independently. (**B**) Schematic diagram of the $MenT_3$ toxin mechanism of action. $MenT_3$ elongates the 3′-CCA motif of specific tRNAs, preventing their charging by aminoacyl-tRNA synthetases (AaRS), thereby interfering with translation and inhibiting bacterial growth.

The fact that $MenT_3$ inhibited protein synthesis, and that RNase PH is involved in the removal of nucleotides following the 3′-CCA sequence required for tRNA aminoacylation, suggested that tRNA charging might be affected by $MenT_3$ expression in vivo. To address this hypothesis, we first used a method developed for *E. coli*, which separates charged from uncharged tRNAs and allows their detection by Northern blot after extraction in vivo (*29*). We chose $tRNA^{Trp}$ as a model tRNA because (i) the tryptophanyl-tRNA can be well separated from uncharged $tRNA^{Trp}$ and (ii) there is only one $tRNA^{Trp}$ in *E. coli* (*29*). No charged tryptophanyl-$tRNA^{Trp}$ could be detected following overexpression of $MenT_3$ when compared to the empty vector control (Fig. 3E and fig. S5E). $tRNA^{Trp}$ charging levels were also investigated in vitro by adding purified $MenT_3$ to the transcription/translation assay described above (Fig. 3E). In this case, $MenT_3$ also affected $tRNA^{Trp}$ charging in vitro, thus supporting the hypothesis that the toxin inhibits protein synthesis by preventing aminoacylation of tRNA.

$MenT_3$ transfers pyrimidines to the 3′ acceptor stem of specific tRNAs

The observation that $MenT_3$ is related to NTases (Fig. 2G) suggests that its mode of action is to directly transfer nucleotides to tRNAs, thereby preventing aminoacylation. We performed assays using

radiolabeled tRNAs to track the addition of nucleotides by $MenT_3$ WT, $MenT_3^{(D80A)}$, and $MenT_3^{(K189A)}$ (Fig. 4).

$MenT_3$ WT was incubated with $tRNA^{Trp}$ from *E. coli*, as a model recipient tRNA, in the presence of guanosine 5′-triphosphate (GTP), adenosine 5′-triphosphate (ATP), uridine 5′-triphosphate (UTP), or cytidine 5′-triphosphate (CTP), and nucleotide transfer was monitored as an increase in tRNA size by high-resolution polyacrylamide gel electrophoresis (PAGE; Fig. 4A). At high concentrations of the enzyme, we found that $MenT_3$ can add two to three extra nucleotides to $tRNA^{Trp}$ in the presence of CTP or UTP, with a slight preference for CTP, suggesting that $MenT_3$ is a pyrimidine-specific NTase (Fig. 4A). No transfer was observed with purines ATP or GTP as substrates (Fig. 4A). $MenT_3^{(D80A)}$, which was unable to inhibit in vitro protein synthesis (fig. S5, A to C), had no NTase activity with either UTP or CTP (Fig. 4B). $MenT_3^{(K189A)}$, which was also inactive in the in vitro transcription/translation assay (fig. S5, A to C), only lost its NTase activity in the presence of UTP, but retained some activity (albeit less than WT) in the presence of CTP, or both nucleotides (Fig. 4C). This could imply that K189A is important for substrate nucleotide selectivity. No synergistic effect was seen when $MenT_3$ WT was incubated with a mixture of CTP and UTP, as the pattern with both nucleotides together resembled that of CTP alone (Fig. 4C).

Canonical tRNA NTases typically add the 3′-CCA motif to tRNAs lacking an encoded 3′-CCA that are processed at the level of the discriminator nucleotide (nucleotide 73). They also repair this motif when 3′-exoribonucleases, such as RNase PH, fail to stop at the 3′-CCA motif when processing tRNA precursors containing an encoded 3′-CCA, typically removing the terminal A residue. Since *M. tuberculosis* contains a mixture of tRNA genes encoding or lacking a 3′-CCA motif, we wondered whether $MenT_3$ had a preference for one class (or another class) of substrate. While faint NTase activity was observed when $MenT_3$ WT and $MenT_3^{(K189A)}$ were incubated with CTP and $tRNA^{Trp}$ lacking a 3′-CCA, the data show that $MenT_3$ had a clear preference for tRNAs that already possessed a 3′-CCA motif (Fig. 4D). This is in contrast to the normal function of tRNA NTases, which prefer tRNAs lacking an intact 3′-CCA. Again, $MenT_3$ WT modified $tRNA^{Trp}$ using both CTP and UTP as substrate, while $MenT_3^{(K189A)}$ could only use CTP (Fig. 4D). Addition of nucleotides to mature tRNAs by $MenT_3$ would completely abolish the ability of these tRNAs to be charged with their cognate amino acid and take part in translation, accounting for their cellular toxicity.

Our in vivo data show that toxins $MenT_3$, as well as $MenT_1$ and $MenT_4$, are significantly less toxic in *E. coli* than in mycobacteria (Fig. 1 and fig. S1), which suggests that these toxins may have a tRNA target preference. We therefore asked whether $MenT_3$ would exhibit some specificity toward the different tRNAs of *M. tuberculosis*. We made polymerase chain reaction (PCR) templates allowing us to in vitro transcribe the 45 different tRNAs of *M. tuberculosis*, each with a 3′-CCA motif (fig. S6). As before, each radiolabeled tRNA was incubated with $MenT_3$ and nonradiolabeled CTP (Fig. 5A). To our surprise, $MenT_3$ appeared to be highly specific, preferentially modifying the four *M. tuberculosis* $tRNA^{Ser}$ isoacceptors, along with weak modification of $tRNA^{Leu5}$ (Fig. 5A). Although we cannot exclude that $MenT_3$ can modify other tRNAs in vivo, the data show that the toxin presents a high degree of specificity toward different tRNAs in vitro, which may explain the variable toxicity observed in different bacteria.

Last, we asked whether the antitoxin $MenA_3$ inhibited the NTase activity of $MenT_3$ directly, or whether it could simply reverse its action by removing the added nucleotides in a manner similar to the RNase PH multicopy suppressor. Addition of $MenA_3$ strongly inhibited the NTase activity of $MenT_3$ on the natural substrate *M. tuberculosis* $tRNA^{Ser2}$ when coincubated with the toxin at a molar ratio > 2.5. However, $MenA_3$ failed to remove the added nucleotides from $tRNA^{Ser2}$ when added after a preincubation of $tRNA^{Ser2}$ with $MenT_3$, even at high concentrations (fig. S7). This suggests that the antitoxin is likely to inhibit the toxin rather than reverse the reaction on the substrate.

DISCUSSION

This study has characterized a family of TA systems from *M. tuberculosis* containing NTase-like DUF1814 toxins, establishing $MenT_3$ as a potent toxin in this problematic pathogen. We have solved the structures of the homologous toxins $MenT_3$ and $MenT_4$ by x-ray crystallography, revealing fold similarity and conserved residues within the proposed active sites, and have observed a similar mode of toxin activity, targeting protein synthesis. We have further elucidated the mechanism of toxicity for $MenT_3$, showing that it functions as a pyrimidine-specific NTase preferentially targeting *M. tuberculosis* $tRNA^{Ser}$ in vitro (Fig. 5B).

The observation that the three NTase toxins identified in this work show different levels of toxicity when expressed in the same host, and that such toxic signatures can vary when expressed in different bacterial hosts (i.e., *E. coli* versus mycobacteria), is intriguing (Fig. 1 and fig. S1). The most marked example is $MenT_1$, which shows robust toxicity in *M. smegmatis* but no toxicity in *E. coli* (Fig. 1A and fig. S1B). Although we cannot exclude this being a result of improper folding or expression of the toxin in *E. coli*, it is also reasonable to assume that the toxin may not be able to recognize its tRNA targets due, for example, to tRNA modification, or the absence of its preferred tRNA target (*30*). Another possibility is that tRNA targets are expressed at higher levels in *E. coli* and are thus sufficiently abundant to overcome the noxious effect of the toxin in vivo. The fact that *M. tuberculosis* and *M. smegmatis* only have 45 and 46 tRNA genes, respectively, while *E. coli* has 86, is in line with this hypothesis (*30*, *31*).

The apparent in vitro specificity of $MenT_3$ for certain *M. tuberculosis* tRNAs, especially $tRNA^{Ser}$, is remarkable (Fig. 5A). We did not test other tRNAs in *E. coli* besides $tRNA^{Trp}$; it may well have been fortuitous that the only tRNA we tested in this organism was detectably modified by the toxin in vitro (Fig. 4A) and in vivo, inferred from the reduced charging levels following toxin expression (Fig. 3E). We checked whether the *M. tuberculosis* tRNAs that were substrates of $MenT_3$ had any distinguishing features and were struck by the fact that all serine tRNAs and several leucine tRNAs were unique among *M. tuberculosis* tRNAs in that they had long variable arms (fig. S8A) (*32*). While this is intriguing and may contribute to substrate specificity, it cannot be the only recognition element because (i) two leucine tRNAs besides $tRNA^{Leu5}$ have variable loops but are not $MenT_3$ substrates in vitro and (ii) *E. coli* $tRNA^{Trp}$ does not have a variable loop (fig. S8B), but can be extended by the NTase activity of the toxin. It is also intriguing in this regard that *M. tuberculosis* $tRNA^{Trp}$ is not a $MenT_3$ substrate in vitro. *E. coli* and *M. tuberculosis* $tRNA^{Trp}$ are highly homologous but do show differences in their variable- and T-arm sequences (fig. S8C). Substrate specificity therefore appears to come from a combination of multiple sequence and structure

motifs. Having identified these tRNA targets in vitro, further work is now needed to confirm targeting in vivo in *M. tuberculosis*.

Our observed TA interactions raise questions regarding the molecular mechanisms of antitoxicity for DUF1814 toxins (fig. S4, C to F). Typically, in type II TA systems, antitoxin function is in part driven by its strong and direct interaction with the cognate toxin (*3*). While we have shown interactions between cognate toxins and antitoxins (fig. S4, C to F), the antitoxin interaction in vivo appears weak. We additionally demonstrated that coincubation of the $MenA_3$ antitoxin with $MenT_3$ is able to neutralize the NTase activity (fig. S7). This suggests that any interaction-based antitoxicity might be a transient and labile mechanism and, due to the difference in size and sequence between antitoxins $MenA_1$ and $MenA_3$ (Fig. 1A), may well differ between these systems.

The DUF4433 DarT toxin from *M. tuberculosis* was recently identified as a single-stranded DNA NTase that specifically and reversibly adenosine 5′-diphosphate (ADP)–ribosylates thymidines (*33*). Our study identifies $MenT_3$ as an NTase toxin from the unrelated DUF1814 protein family. In comparison to DarT, $MenT_3$ acts via a distinct and novel mode of toxicity where the $MenT_3$ toxin preferentially targets *M. tuberculosis* tRNAs in vitro, preventing their charging with cognate amino acids by adding nucleotides to the 3′-CCA acceptor stem (Fig. 5B). Accordingly, antitoxin function also appears to differ between these systems. Whereas DarT is counteracted enzymatically by the cognate antitoxin DarG via target de-ADP-ribosylation (*33*), we found that $MenA_3$ was unable to reverse $MenT_3$ toxicity by removing nucleotides, suggesting that $MenA_3$ likely inhibits the toxin activity.

Increasing numbers of toxins have been identified that target tRNAs by various mechanisms (*13*). The *M. tuberculosis* type II VapC toxins function as endoribonucleases cleaving tRNAs (*34*), whereas TacT from *Salmonella* Typhimurium and AtaT from *E. coli* are tRNA acetyltransferases, modifying charged tRNAs to block translation (*35*, *36*). That $MenT_3$ provides yet another way to inhibit tRNA activity is perhaps not unusual, given the essential nature of translation to cellular growth and survival. This likely reflects the value of possessing multiple TA systems to promote adaptability to different stressful environments via tRNA metabolism, with downstream effects ranging from stalling cell growth to potentially altering translation output (*13*). It remains to be seen whether this mechanism is conserved among DUF1814-toxins; while $MenT_4$ shares structural similarities to $MenT_3$ and inhibits protein synthesis in vitro (Fig. 2 and fig. S5D), we have not yet explored the molecular mechanism behind its toxicity. Given the continued significance of *M. tuberculosis* worldwide, the mechanism used by the $MenA_3$-$MenT_3$ TA system highlights a new way to block protein synthesis. We propose that further exploring the molecular mechanisms of both toxicity and antitoxicity will provide useful insights into the regulation of bacterial growth.

MATERIALS AND METHODS

Bacterial strains and culture conditions

E. coli DH5α (Invitrogen), DH10B (Thermo Fisher Scientific), BL21 (λDE3) (Novagen), ER2566 (New England Biolabs), W3110 [strain American Type Culture Collection (ATCC) 27325], DLT1900 (*37*), and *M. smegmatis* mc^2 155 (strain ATCC 700084) are as previously described. To construct BL21 (λDE3) Δ*slyD*, the Δ*slyD*::Km^R allele from JW3311 (Keio collection) was moved into BL21 (λDE3) using bacteriophage P1-mediated transduction. To construct the unmarked DLT1900 Δ*rph* mutant, the Δ*rph*::Km^R allele from JW3618 (Keio collection) was first moved into DLT1900 using bacteriophage P1-mediated transduction and by subsequent removing of the kanamycin (Km) resistance cassette using plasmid pCP20, as previously described (*38*). *E. coli* were routinely grown at 37°C in LB medium or M9 minimal (M9M) medium supplemented when necessary with Km (50 μg ml^{-1}), ampicillin (Ap; 50 μg ml^{-1}), chloramphenicol (Cm; 34 μg ml^{-1}), streptomycin (Sm; 25 μg ml^{-1}), spectinomycin (Sp; 50 μg ml^{-1}), IPTG (1 mM), L-ara (0.1% w/v), or D-glucose (glu; 0.2% w/v). *M. smegmatis* mc^2 155 strains were routinely grown at 37°C in either LB or 7H9 medium (Difco). *M. tuberculosis* H37Rv (WT; ATCC 27294) and mutant strains were routinely grown at 37°C in complete 7H9 medium (Middlebrook 7H9 medium, Difco) supplemented with 10% albumin-dextrose-catalase (ADC; Difco) and 0.05% Tween 80 (Sigma-Aldrich), or on complete 7H11 solid medium (Middlebrook 7H11 agar medium, Difco) supplemented with 10% oleic acid–ADC (OADC; Difco). When required, mycobacterial growth media were supplemented with Km (50 μg ml^{-1}), hygromycin (Hm; 50 μg ml^{-1}), Sm (25 μg ml^{-1}), zeocin (Zc; 25 μg ml^{-1}), Ace (0.2% w/v), or Atc (100 or 200 ng ml^{-1}).

Plasmid constructs

Plasmids pMPMK6 (*39*), p29SEN (*40*), pGMCS (*41*), pGMCZ (*42*), pLAM12 (*43*), pETDuet-1, pET15b and pRARE (Novagen), pBAD30 (*44*), and pTA100 (*4*) have been described. Primers used for plasmid construction are described in table S1. All the plasmids constructed in this work have been verified by sequencing. The pMPMK6 derivatives expressing the toxins, namely, pK6-$MenT_1$, pK6-$MenT_2$, pK6-$MenT_3$, and pK6-$MenT_4$, were constructed as follows: *menT*$_1$, *menT*$_2$, *menT*$_3$, and *menT*$_4$ were PCR-amplified from the *M. tuberculosis* H37Rv genome and cloned as Eco RI/Hind III fragments (*menT*$_1$ and *menT*$_2$) and Mfe I/Hind III fragments (*menT*$_3$ and *menT*$_4$) into Eco RI/Hind III–digested pMPMK6.

The p29SEN plasmid derivatives encoding the antitoxins, namely, p29SEN-$MenA_1$, p29SEN-$MenA_2$, p29SEN-$MenA_3$, and p29SEN-$MenA_4$, were constructed as follows: *menA*$_1$, *menA*$_2$, *menA*$_3$, and *menA*$_4$ were PCR-amplified from the *M. tuberculosis* H37Rv genome and cloned either as Eco RI/Hind III fragments (*menA*$_1$, *menA*$_2$, and *menA*$_3$) or as Mfe I/Hind III fragments (*menA*$_4$) into Eco RI/Hind III–digested p29SEN. For p29SEN-Rph, the *rph* gene was PCR-amplified from the *E. coli* DLT1900 genome and cloned as an Eco RI/Hind III fragment into Eco RI/Hind III–digested p29SEN.

To construct pGMC-$MenT_2$, pGMC-$MenT_3$, and pGMC-$MenT_4$, *menT*$_2$, *menT*$_3$, and *menT*$_4$ were PCR-amplified using pK6-$MenT_2$, pK6-$MenT_3$, and pK6-$MenT_4$ templates, respectively, and cloned into pGMCS using In-Fusion HD Cloning Kits (Takara Bio). Plasmid pGMC-$MenT_1$ and pGMC-$MenT_{1\text{-}His}$ were obtained following PCR amplification of *menT*$_1$ and *menT*$_{1\text{-}His}$ using pK6-$MenT_1$ as a template and homologous recombination in linearized pGMCS plasmid by In-Fusion HD Cloning Kits (Takara Bio). For pGMC-*$MenA_4$-$MenT_4$, the *menA*$_4$-*menT*$_4$ operon was PCR-amplified from the H37Rv genome and cloned into linearized pGMCS plasmid by In-Fusion HD Cloning Kits (Takara Bio).

To construct plasmids pLAM-$MenA_2$, pLAM-$MenA_3$, and pLAM-$MenA_4$, *menA*$_2$, *menA*$_3$, and *menA*$_4$ were PCR-amplified using p29SEN-$MenA_2$, p29SEN-$MenA_3$, and p29SEN-$MenA_4$ as templates, respectively. These were cloned as Nde I/Eco RI fragments (*menA*$_2$ and *menA*$_3$) and Nde I/Mfe I fragments (*menA*$_4$) into Nde I/Eco

RI–digested pLAM12. Plasmid p29SEN-MenA$_1$ was used to amplify *menA$_1$* and *menA$_{1\text{-}His}$*, which were then cloned as Nde I/Eco RI fragments into Nde I/Eco RI–digested pLAM12 to produce pLAM-MenA$_1$ and pLAM-MenA$_{1\text{-}His}$, respectively.

The pET vector derivatives used in this work were constructed as follows. To construct plasmid pET-MenT$_{3\text{-}His}$, *menT$_{3\text{-}His}$* (with an added fragment encoding a Ser-Ser-Gly-His$_6$ C-terminal tag) was PCR-amplified from pK6-MenT$_3$ template and cloned as an Nde I/Mfe I fragment into Nde I/Mfe I–digested pETDuet-1. Plasmid pET-MenT$_{3\text{-}His}$ was used as a template to construct pET-MenT$_{3\text{-}His}^{(D80A)}$ and pET-MenT$_{3\text{-}His}^{(K189A)}$ by QuikChange site-directed mutagenesis (Agilent) using appropriate primers. Plasmid pET-MenA$_{3\text{-}His}$, encoding an N-terminal His$_6$-tagged MenA$_3$ antitoxin, was constructed by PCR amplification of *menA$_{3\text{-}His}$* using p29SEN-MenA$_3$ as a template, Nde I/Hind III digestion, and cloning into Nde I/Hind III–digested pET15b plasmid. To construct plasmid pET-MenT$_3$/MenA$_{3\text{-}His}$, *menA$_{3\text{-}His}$* was first PCR-amplified from p29SEN-MenA$_3$ template and cloned as an Nco I/Hind III fragment into Nco I/Hind III–digested pETDuet-1. *menT$_3$* was then PCR-amplified from pK6-MenT$_3$, digested with Nde I/Mfe I, and cloned into Nde I/Mfe I–digested pET-MenA$_{3\text{-}His}$. To construct pET-MenT$_{3\text{-}His}$/MenA$_3$, *menA$_3$* was first PCR-amplified using p29SEN-MenA$_3$ as a template and cloned as an Nco I/Hind III fragment into Nco I/Hind III–digested pET-MenT$_{3\text{-}His}$. To generate pET-MenT$_{1\text{-}His}$ (expressing MenT$_1$ with an N-terminal His$_6$-Ser-Ser-Gly-tag), *menT$_{1\text{-}His}$* was PCR-amplified from pK6-MenT$_1$ and cloned as an Nde I/Mfe I fragment into Nde I/Mfe I–digested pETDuet-1. For pET-MenA$_{1\text{-}His}$ (expressing MenA$_1$ with an N-terminal His$_6$-Ser-Ser-Gly-tag), *menA$_{1\text{-}His}$* was PCR-amplified from p29SEN-MenA$_1$ template and cloned as an Nco I/Bam HI fragment into Nco I/Bam HI–digested pETDuet-1. For pET-MenT$_1$/MenA$_{1\text{-}His}$, *menT$_1$* was PCR-amplified from pK6-MenA$_1$ and cloned as an Nde I/Mfe I fragment into Nde I/Mfe I–digested pET-MenA$_{1\text{-}His}$. For pET-MenT$_{1\text{-}His}$/MenA$_1$, *menA$_1$* was PCR-amplified from p29SEN-MenA$_1$ and cloned as an Nco I/Bam HI fragment into Nco I/Bam HI–digested pET-MenT$_{1His}$.

To generate MenT$_3$ and MenT$_4$ expression constructs for crystallization and biochemistry, overlap PCRs were performed to fuse a sentrin protease (SENP)–cleavable N-terminal His$_6$-SUMO tag, amplified from the pBAT4 derivative (*45*), pSAT1-LIC (this study), to either *menT$_3$* or *menT$_4$*, amplified from H37Rv genomic DNA. The resulting PCR products were cloned as either Kpn I/Hind III fragments into Kpn I/Hind III–digested pBAD30 (*menT$_3$*), producing pTRB517, or as Xma I/Hind III fragments into Xma I/Hind III–digested pBAD30 (*menT$_4$*) to generate pTRB544.

Plasmids pPF656 and pPF657 were constructed by amplifying *menA$_3$* and *menT$_3$* from H37Rv genomic DNA and cloning as Mfe I/Xma I fragments into Eco RI/Xma I–digested pTA100 and pBAD30, respectively. To express His$_6$-SUMO-tagged MenT$_3^{(D80A)}$, site-directed mutagenesis was carried out using pTRB517 as a template. Briefly, nonoverlapping inverse primers were used to amplify *menT$_3^{(D80A)}$*, followed by incubation with a mix of T4 DNA ligase, T4 polynucleotide kinase, and DpnI at 37°C to remove template and circularize amplified DNA. This reaction was then used to transform *E. coli* DH5α, resulting in pTRB593. Similarly, this method was used to generate MenT$_3^{(D80A)}$, MenT$_3^{(K189A)}$, and MenT$_3^{(D211A)}$ for functional testing, using pPF657 as a template, resulting in pTRB591, pTRB562, and pTRB592, respectively.

Plasmid pTRB491 was generated by amplifying *menA$_3$* from H37Rv genomic DNA and cloning into pSAT1-LIC via ligation-independent cloning (LIC). The pSAT1-LIC plasmid features a LIC site that fuses an N-terminal His$_6$-SUMO tag to the target protein. To produce MenT$_3^{(K189A)}$ protein, the mutated gene was amplified from pTRB562 and similarly cloned into pTRB550 via LIC, resulting in pTRB577. The pTRB550 plasmid features a His$_6$-SUMO LIC site, originally amplified from pSAT1-LIC and cloned as an Eco RI/Hind III fragment into Eco RI/Hind III–digested pBAD30.

To produce plasmids for use in *M. tuberculosis*, *menA$_3$*, *menT$_3$*, or both genes were amplified by PCR using PrimeSTAR GXL DNA polymerase, with *M. tuberculosis* H37Rv genomic DNA as template and primer pairs clo-RBS1-MenA$_3$-attB2/clo-MenA$_3$-attB3, clo-RBS1-MenT$_3$-attB2/clo-MenT$_3$-attB3, clo-RBS4-MenT$_3$-attB2/clo-MenT$_3$-attB3, or clo-RBS1-MenA$_3$-attB2/clo-MenT$_3$-attB3, respectively (tables S1 and S2). RBS1 (AGGAAGACAGGCTGCCC) and RBS4 (ACGAAGACAGGCTGCCC), corresponding to a strong or weak Shine-Dalgarno sequence, respectively, were placed upstream from the ATG translation start of MenA$_3$ or the GTG translation start of MenT$_3$. Plasmids pGMCS-TetR-P1-RBS1-MenA$_3$, pGMCS-TetR-P1-RBS1-MenA$_3$-MenT$_3$, pGMCS-TetR-P1-RBS1-MenT$_3$, or pGMCS-TetR-P1-RBS4-MenT$_3$ were constructed by multisite gateway recombination (*18*), using plasmid pDE43-MCS as the destination vector. These plasmids are integrative vectors (insertion at the attL5 mycobacteriophage insertion site in the *glyV* tRNA gene) and express MenA$_3$, MenT$_3$, or MenA$_3$-MenT$_3$ under the control of P1 (P$_{mycl\ tetO}$), a tetracycline-inducible promoter (table S2) (*46*).

Construction of MenT$_3$ D80A, D211A, and K189A substitutions for use in *M. tuberculosis* was performed as follows: Plasmid pGMCS-TetR-P1-RBS4-MenT$_3$ was amplified by PCR with PrimeSTAR GXL DNA polymerase and the oligonucleotides pairs InFus-MenT$_3$D80A-right/InFus-MenT$_3$D80A-left, InFus-MenT$_3$D211A-right/InFus-MenT$_3$D211A-left, or InFus-MenT$_3$K189A-right/InFus-MenT$_3$K189A-left (table S1). The amplified linear fragments were purified on agarose gels and circularized using the In-Fusion HD Cloning Kit (Takara), as recommended by the manufacturer. Plasmids used to transform Stellar recipient cells were verified by sequencing and introduced by electroporation into *M. tuberculosis* Δ(*menA$_3$-menT$_3$*)::*dif6*/pGMCZ (see the next paragraph).

Construction of *M. tuberculosis* mutants

Mutant strains of *M. tuberculosis* H37Rv were constructed by allelic exchange using recombineering (*43*), as previously described (fig. S2) (*47*). Two ~0.5-kb DNA fragments flanking the *menA$_3$-menT$_3$* operon were amplified by PCR using PrimeSTAR GXL DNA polymerase (Takara), *M. tuberculosis* H37Rv genomic DNA, and the primer pairs MenA$_3$Am-For/MenA$_3$Zc-Am-Rev or MenT$_3$Zc-Av-For/MenT$_3$Av-Rev, respectively (table S1). A three-fragment PCR fused these two fragments to a Zc-resistance cassette flanked by two *dif6* variants of the *M. tuberculosis dif* site and the recombination substrate was recovered by agarose gel purifications. The recipient strain for recombineering was a derivative of *M. tuberculosis* H37Rv carrying two plasmids: pJV53H, an Hm-resistant pJV53-derived plasmid expressing recombineering enzymes (*43*), and the integrative plasmid pGMCS-P1-MenA$_3$, constitutively expressing *menA$_3$* (table S2). This strain was grown in complete 7H9 medium supplemented with Hm until mid-log phase and expression of recombineering enzymes was induced by Ace (0.2%) overnight at 37°C. After induction, electrotransformation was performed with 100 ng of the linear DNA fragment for allelic exchange. After a 48-hour incubation at 37°C, mycobacteria were plated onto agar supplemented

with Zc. Zc-resistant clones were restreaked on the same medium, grown in complete 7H9 without antibiotic, and verified to be carrying the expected allele replacement by PCR amplification of chromosomal DNA and subsequent DNA sequencing, using primers $MenA_3$Am-For/$MenT_3$Av-Rev (fig. S1C and table S1). Spontaneous loss of the Zc-resistance cassette by XerCD-dependent recombination and of the pJV53H plasmid was obtained by serial rounds of culture without antibiotics and phenotypic tests for Zc^S and Hm^S. Plasmid pGMCS-P1-$MenA_3$ was then removed by transformation with pGMCZ, a similar integrative vector but carrying resistance to Zc, resulting in the deleted strain *M. tuberculosis* Δ(*$menA_3$-$menT_3$*)::*dif*6/pGMCZ.

E. coli multicopy plasmid library

E. coli MC4100 Δ*dnaKdnaJ*::Km^R Δ*tig*::Cm^R double mutant (*40*) was partially digested with Sau3 AI restriction enzyme and DNA fragments of about 1.5 to 4 kb in size were purified, then ligated into linearized and dephosphorylated Bam HI–digested pMPM2 (ColE1 origin) plasmid (*39*), and used to transform *E. coli* DH10B. About 25,000 independent transformants were pooled to constitute the multicopy library. This library has previously been used as a tool to identify multicopy suppressors of chaperone mutants (*48*).

Bacterial growth assays

In vivo toxicity and antitoxicity assays by cognate or noncognate antitoxins in *E. coli* were performed as follows. *E. coli* DLT1900 were cotransformed with pMPMK6-vector, pK6-$MenT_1$, -$MenT_2$, -$MenT_3$, or -$MenT_4$ (toxins), and p29SEN-vector, p29SEN-$MenA_1$, -$MenA_2$, -$MenA_3$, or -$MenA_4$ (antitoxins). Transformants were re-seeded from overnight cultures and grown at 37°C to mid-log phase in LB supplemented with Km and Ap, and then serially diluted and spotted on LB-agar plates supplemented with Km and Ap, with or without L-ara (0.1%) and/or IPTG (200 μM). Plates were incubated at 37°C overnight and then imaged and counted. $MenT_3$ substitutions were tested for toxicity in *E. coli* DH5α carrying pBAD30-vector, -$MenT_3$ WT (pPF657), -$MenT_3^{(D80A)}$ (pTRB591), -$MenT_3^{(K189A)}$ (pTRB562), or -$MenT_3^{(D211A)}$ (pTRB592). Strains were grown to mid-log phase, then serially diluted, and spotted onto M9M-agar plates supplemented with Ap, with or without L-ara (0.1%). After a 2-day incubation at 37°C, plates were imaged and counted.

In vivo toxicity and rescue assays by cognate or noncognate antitoxins in *M. smegmatis* were performed as follows. Cultures of mc^2 155 strain grown in LB at 37°C were cotransformed with the integrative pGMC-vector, -$MenT_1$, -$MenT_2$, -$MenT_3$, or -$MenT_4$ (toxins), and with pLAM12-vector, pLAM-$MenA_1$, -$MenA_2$, -$MenA_3$, or -$MenA_4$ (antitoxins). Samples were selected on LB-agar plates supplemented with Km and Sm for 3 days at 37°C, in the presence or absence of Atc (100 ng ml^{-1}) and Ace (0.2%) for toxin and antitoxin expression, respectively. A similar procedure was applied for pGMC-*$MenA_4$-$MenT_4$ carrying the *$menA_4$-$menT_4$* operon, with the exception that no cotransformation with pLAM12 derivatives or selection on Km was needed.

Viability staining and flow cytometry

Exponentially growing cultures [OD_{600} (optical density at 600 nm) between 0.05 and 0.2] of *M. smegmatis* strain mc^2 155 containing plasmid pGMCS-TetR-P1-RBS1-$MenT_3$ were divided in two: Half was left in complete 7H9 growth medium with Sm (uninduced cultures), while the other half was additionally treated with Atc (200 ng ml^{-1}) to induce expression from the P1 promoter. For labeling with LIVE/DEAD BacLight (Molecular Probes) dyes, cells were harvested 8 hours after Atc induction. Cells were centrifuged, resuspended in phosphate-buffered saline buffer, and stained as recommended by the manufacturer. Labeled cells were analyzed by fluorescence-activated cell sorting using a BD LSRFortessa X20 flow cytometer. Flow cytometry data analysis was performed using FlowJo software.

Toxicity assays in *M. tuberculosis*

M. tuberculosis strains H37Rv or H37Rv Δ(*$menA_3$-$menT_3$*)::*dif*6/pGMCZ were transformed by electroporation with 100 ng of plasmids pGMCS-TetR-P1-RBS1-$MenA_3$, pGMCS-TetR-P1-RBS1-$MenA_3$-$MenT_3$, pGMCS-TetR-P1-RBS1-$MenT_3$, pGMCS-TetR-P1-RBS4-$MenT_3$, pGMCS-TetR-P1-RBS4-$MenT_3$(D80A), pGMCS-TetR-P1-RBS4-$MenT_3$(K189A), or pGMCS-TetR-P1-RBS4-$MenT_3$(D211A). After 3 days of phenotypic expression in 7H9 ADC Tween at 37°C, the transformation mix was divided into two halves. One half was plated on 7H11 OADC with Sm; the other half was plated on 7H11 OADC Sm supplemented with Atc (200 ng ml^{-1}). Plates were imaged after 20 days of incubation at 37°C.

In vivo coaffinity purification assays

To perform in vivo copurification assays, *E. coli* BL21 Δ*slyD* was transformed with (i) pET-$MenT_{3\text{-His}}$, pET-$MenA_{3\text{-His}}$, pET-$MenT_3$/$MenA_{3\text{-His}}$, or pET-$MenT_{3\text{-His}}$/$MenA_3$, or with (ii) pET-$MenT_{1\text{-His}}$, pET-$MenA_{1\text{-His}}$, pET-$MenT_1$/$MenA_{1\text{-His}}$, or pET-$MenT_{1\text{-His}}$/$MenA_1$, and selected on LB-agar plates supplemented with Ap and glu (20%). Transformants were grown at 37°C to an OD_{600} of approximately 0.4 and then protein expression was induced overnight at 20°C with 1 mM IPTG. Cell lysis and affinity purification of the protein complexes were performed as described below for $MenT_{3\text{-His}}$ purification. Elution fractions were separated on SDS-PAGE and proteins revealed using InstantBlue Protein Stain (Expedeon, catalog no. ISB1L).

Recombinant protein production

To purify $MenT_3$ for biochemistry, BL21 (λDE3) Δ*slyD* transformed with pET-$MenT_{3\text{-His}}$, pET-$MenT_{3\text{-His}}^{(D80A)}$, or pET-$MenT_{3\text{-His}}^{(K189A)}$ was grown to an OD_{600} of approximately 0.4 at 37°C. IPTG (1 mM) was then added, and the culture was incubated overnight at 20°C. Under such conditions, $MenT_3$ expression in *E. coli* was better tolerated and led to a reasonable amount of soluble $MenT_3$ that could be collected for purification. Cultures were centrifuged at 5000*g* for 10 min at 4°C, pellets were resuspended in Lysis buffer [300 mM NaCl, 50 mM tris (pH 7.5), and protease inhibitor tablet (Roche); 20 ml of buffer per 1 liter of cell culture] and incubated for 30 min on ice. Lysis was performed using the One Shot cell disrupter at 1.5 kbar (One Shot model, Constant Systems Ltd.). Lysates were centrifuged for 30 min at 30,000*g* in 4°C, and the resulting supernatants were gently mixed at 4°C for 30 min with Ni–nitrilotriacetic acid agarose beads (Qiagen, catalog no. 30230) preequilibrated with buffer PD [300 mM NaCl and 50 mM tris (pH 7.5)], using a 10-ml poly-prep column (Bio-Rad, catalog no. 7311550). Columns were stabilized for 10 min at 4°C and washed three times with 10 ml of buffer PD plus 25 mM imidazole, and proteins were then eluted with buffer PD containing 250 mM imidazole. Elutions (500 μl) were collected and PD MiniTrap G-25 columns (GE Healthcare, catalog no. 16924748) were used to exchange buffer with buffer PD

supplemented with 10% glycerol. Proteins were concentrated using Vivaspin 6 columns with a 5000-Da cutoff (Sartorius, catalog no. 184501257). Proteins were stored at −80°C until further use.

For additional $MenT_3$ and $MenT_3^{(K189A)}$ expression, either for crystallization or biochemistry, *E. coli* ER2566 pRARE pPF656 was transformed with either pTRB517 or pTRB577, respectively. For $MenT_3^{(D80A)}$ expression, *E. coli* ER2566 pRARE was transformed with pTRB593. $MenT_4$ was expressed in *E. coli* BL21 (λDE3) transformed with pTRB544. $MenA_3$ was expressed in *E. coli* ER2566 transformed with pTRB491. For these expressions, the same procedure was followed: Overnight cultures were re-seeded 1:100 into 2-liter flasks containing 1-liter 2× YT. Cells were grown at 175 rpm in 37°C until an OD_{600} of 0.3 was reached and then at 22°C until OD_{600} 0.5, whereupon expression was induced by the addition of L-ara (0.1%) for toxins and IPTG (1 mM) for antitoxins. Cells were left to grow overnight at 16°C, shaking at 175 rpm.

For selenomethionine incorporation, starter cultures of ER2566 pRARE pPF656 pTRB517 were grown overnight in LB at 37°C with 200 rpm shaking. Cells were pelleted, washed, and resuspended in M9M, and then sub-cultured into 500 ml of M9M in 2-liter baffled flasks to a starting OD_{600} of 0.075. Cells were grown at 37°C with 175 rpm shaking until an OD_{600} of 0.6, whereupon cells were centrifuged at 4200*g* and resuspended in fresh M9M. This sample was divided between separate 2-liter baffled flasks containing new M9M and shaken at 175 rpm for a further 1 hour at 37°C. Once an OD_{600} of 0.7 was reached, 12 ml of nutrient mix [L-lysine hydrate (4 mg ml^{-1}), L-threonine (4 mg ml^{-1}), L-phenylalanine (4 mg ml^{-1}), L-leucine (2 mg ml^{-1}), L-isoleucine (2 mg ml^{-1}), L-valine (2 mg ml^{-1}), and 4 mM $CaCl_2$] was added to each flask to promote feedback inhibition of methionine synthesis, followed by 250× SelenoMethionine Solution (Molecular Dimensions) to a final concentration of 40 μg ml^{-1}, and cells were left to incubate for 1 hour at 20°C. Last, toxin and antitoxin expression were induced by the addition of L-ara (0.1%) and IPTG (1 mM), and samples were left to grow overnight at 175 rpm in 16°C.

All five proteins were purified in the same manner. Bacteria were harvested by centrifugation at 4200*g*, and the pellets were resuspended in buffer A500 [20 mM tris-HCl (pH 7.9), 500 mM NaCl, 5 mM imidazole, and 10% glycerol]. Cells were lysed by sonication at 40 kpsi and then centrifuged (45,000*g*, 4°C). The clarified lysate was next passed over a HisTrap HP column (GE Healthcare), washed for 10 column volumes with A500, followed by 10 column volumes of buffer A100 [20 mM tris-HCl (pH 7.9), 100 mM NaCl, 5 mM imidazole, and 10% glycerol], and then eluted directly onto a HiTrap Q HP column (GE Healthcare) with buffer B100 [20 mM tris-HCl (pH 7.9), 100 mM NaCl, 250 mM imidazole, and 10% glycerol]. The Q HP column was transferred to an Äkta Pure (GE Healthcare), washed with 3 column volumes of A100, and then proteins were eluted using a gradient from 100% A100 to 100% buffer C1000 [20 mM tris-HCl (pH 7.9), 1000 mM NaCl, and 10% glycerol]. Fractions containing the protein peak were analyzed by SDS-PAGE, pooled, and incubated overnight at 4°C with hSENP2 SUMO protease to cleave the His_6-SUMO tag from the target protein. The following day, the samples were passed through a second HisTrap HP column and the flow-through fractions containing untagged target protein were collected. These samples were concentrated and run over a HiPrep 16/60 Sephacryl S-200 size exclusion column (GE Healthcare) in buffer S [50 mM tris-HCl (pH 7.9), 500 mM KCl, and 10% glycerol]. Peak fractions were analyzed by SDS-PAGE, pooled, and concentrated. Optimal fractions were separated and either flash-frozen in liquid N_2 for storage at −80°C or dialyzed overnight at 4°C into buffer X [20 mM tris-HCl (pH 7.9), 150 mM NaCl, and 2.5 mM dithiothreitol (DTT)] for crystallographic studies. Crystallization samples were quantified and stored on ice and then either used immediately or flash-frozen in liquid N_2 for storage at −80°C. Frozen crystallization samples still formed usable crystals 15 months after storage.

Protein crystallization

Native and selenomethionine-derivatized $MenT_3$ were concentrated to 12 mg ml^{-1} and $MenT_4$ was concentrated to 6 mg ml^{-1}, all in buffer X (see above). Initial crystallization screens were performed using a Mosquito Xtal3 robot (TTP Labtech) to set 200:100 nl and 100:100 nl protein:condition sitting drops. After initial screening and optimization, both $MenT_3$ protein samples formed thick, six-sided needles in condition G5 [0.2 M calcium acetate hydrate, 0.1 M tris (pH 8.5), and 25% w/v polyethylene glycol 2000 monomethyl ether] of Clear Strategy II HT-96 (Molecular Dimensions). $MenT_4$ formed thin, six-sided needles in the same condition as $MenT_3$. To harvest, 20 μl of condition reservoir was added to 20 μl of cryo buffer [25 mM tris-HCl (pH 7.9), 187.5 mM NaCl, 3.125 mM DTT, and 80% glycerol] and mixed quickly by vortexing; an equal volume of this mixture was then added to the drop. After addition of cryo buffer, crystals were immediately extracted using a nylon loop and flash-frozen in liquid N_2.

Data collection and structure determination

Diffraction data were collected at Diamond Light Source on beamlines I04 ($MenT_3$ native), I03 ($MenT_3$ selenomethionine-derivatized), and I24 ($MenT_4$ native) (Table 1). Single 360° datasets were collected for native $MenT_3$ and $MenT_4$. Two 360° datasets from $MenT_3$ selenomethionine-derivatized crystals measured at the selenium peak (0.9793 Å) were merged using iSpyB (Diamond Light Source). Additional $MenT_3$ selenomethionine-derivatized datasets were collected at selenium high remote (0.9641 Å) and inflection (0.9795 Å) wavelengths. Diffraction data were processed with XDS (*49*), and then AIMLESS from CCP4 (*50*) was used to corroborate the space groups (Table 1). The crystal structure of $MenT_3$ was solved by MAD by providing the SHELX suite in CCP4 with the native and three anomalous $MenT_3$ datasets. The solved starting model for $MenT_3$ was built in REFMAC within CCP4. The crystal structure of $MenT_4$ was solved ab initio using ARCIMBOLDO (*51*). Both models were then iteratively refined and built using PHENIX (*52*) and COOT (*53*), respectively. The quality of the final model was assessed using COOT and the wwPDB validation server. Structural figures were generated using PyMOL (Schrödinger). Comparison against models within the Protein Data Bank (PDB) was performed using DALI (*25*).

Genetic screen for suppressors of toxicity

The following genetic procedure was developed and applied to select for *E. coli* genes that confer resistance to the $MenT_3$ toxin. *E. coli* strain DLT1900 was first transformed with pK6-$MenT_3$ (Km^R) plasmid and transformants were selected at 37°C on LB-agar plates supplemented with Km and glu (0.2%) to repress toxin expression from the *araBAD* promoter of pK6-$MenT_3$. DLT1900 containing pK6-$MenT_3$ was then grown in LB supplemented with Km and glu, transformed with the pMPMA2-based multicopy library of *E. coli* genes, and plated on selective LB-agar supplemented with Km, Ap, and L-ara (0.1%) to induce toxin expression. Plates were incubated for 24 hours at 37°C. A control aliquot of transformants plated on nonselective plates (no L-ara) indicated that the number of

transformants tested during the selection procedure was approximately 60,000. Note that under such conditions, *E. coli* DLT1900 pK6-MenT$_3$ transformed with pMPMA2 empty vector did not produce any colonies on selective plates. We identified 72 toxin-resistant colonies that grew on selective plates after 24 hours, although they were smaller and translucent, indicating that growth inhibition by the toxin is not fully blocked by the suppressors identified. Of the 72 toxin-resistant colonies identified, only 41 were able to grow in culture. Plasmids were extracted from the 41 cultures, used to re-transform DLT1900 pK6-MenT$_3$, and plated as above, to validate growth rescue in the presence of MenT$_3$. Of 41 clones, 18 suppressors passed the second round of selection and were sequenced using the pMPMA2-For and -Rev primers (table S1).

In vitro transcription/translation assays

Assays were performed as previously described (*54*). Briefly, template DNAs of DHFR (P0ABQ4), WaaF-Strep (P37692), and GatZ-Strep (P0C8J8) were used for in vitro transcription/translation coupled assays (PURExpress, New England Biolabs). These were performed according to the manufacturer's instructions, in the presence or absence of the toxin. Following protein synthesis reactions of 2 hours at 37°C, samples were separated on SDS-PAGE and visualized by InstantBlue staining (DHFR) or Western blots using anti-Strep tag antibodies (WaaF-Strep and GatZ-Strep).

Identification of uncharged tRNAs in vivo and in vitro

Prevention of *E. coli* tRNA^{Trp} aminoacylation by MenT$_3$ was monitored using a combination of two previously published methods (*29*, *55*). *E. coli* BL21 (λDE3) transformed with pETDuet or pET-MenT$_3$ was grown at 37°C to OD_{600} 0.1 in M9M, whereupon expression of MenT$_3$ was induced with 1 mM IPTG until an OD_{600} of about 0.4. The bacterial culture (25 ml) was then kept on ice and centrifuged for 10 min at 5000*g* in 4°C. The pellet was resuspended in 0.5 ml of cold 0.3 M sodium acetate (pH 4.5) and 10 mM EDTA and transferred to a precooled 1.5-ml microcentrifuge tube, and 0.5 ml of phenol (equilibrated with the same buffer) was then added. After gentle pipetting, the sample was transferred into phase-lock tubes with an additional 400 μl of cold chloroform. After 30 seconds shaking, the sample was first incubated on ice for 15 min and then centrifuged for 20 min at 20,000*g* in 4°C. The aqueous phase was then transferred to a new cold 1.5-ml tube. Five hundred microliters of cold isopropanol was added and immediately mixed. RNA was precipitated for 1 hour at −20°C, before the sample was centrifuged for 30 min at 20,000*g* in 4°C (*55*). The supernatant was discarded and 1 ml of cold 75% ethanol was carefully added without disturbing the RNA pellet. After further centrifugation for 10 min at 20,000*g* in 4°C, the supernatant was removed and the pellet was air-dried until no ethanol remained. The pellet was then resuspended by vigorously mixing in 20 μl of cold 10 mM sodium acetate (pH 4.5) and 1 mM EDTA. Samples were stored at −80°C. Samples were separated on a denaturing urea acrylamide gel for 3 hours at 100 V in 4°C, as previously described (*29*). Northern blot and visualization with a radiolabeled DNA probe against tRNA^{Trp} was performed as previously described (*56*). Note that to distinguish the band of aminoacylated tRNA from its deacylated counterpart on the Northern blot, a chemically deacylated aliquot of RNA sample prepared from strain containing the empty vector was subjected to alkaline treatment. In this case, 46 μl of tris-HCl (pH 9.0) was added to a 4-μl aliquot of the RNA sample and incubated for 2 hours at 37°C. Fifteen microliters of 0.3 M sodium acetate at pH 4.5 was added and followed by 125 μl of 96% ethanol. RNA was precipitated at −20°C for 1 hour, resuspended, and separated as described above.

For in vitro tRNA charging, in vitro transcription/translation assays were performed as above, using *gatZ* as DNA template. After a 2-hour reaction at 37°C with or without MenT$_3$ toxin (10 μM), tRNA extraction, separation, and visualization were performed as described for the in vivo samples.

In vitro transcription of tRNAs

Labeled tRNAs were prepared by in vitro transcription of PCR templates containing an integrated T7 RNA polymerase promoter sequence. The template for *E. coli* tRNA^{Trp} was made by PCR amplification of chromosomal DNA from strain MG1655 with the primers CC2556 and CC2557 (CC2591 for tRNA^{Trp} without CCA) (table S1). The oligos for *M. tuberculosis* tRNAs are given in table S1. The T7 RNA polymerase in vitro transcription reactions were performed in 25-μl total volume, with a 5-μl nucleotide mix of 2.5 mM ATP, 2.5 mM CTP, 2.5 mM GTP, and 60 μM UTP and 2 to 4 μl of 10 mCi ml^{-1} of radiolabeled UTP [α-P^{32}]. Template (0.1 to 0.2 μg) was used per reaction with 1.5 μl of rRNasin (40 U ml^{-1}) (Promega), 5 μl of 5× optimized transcription buffer (Promega), 2 μl of T7 RNA polymerase (20 U ml^{-1}), and 2.5 μl of 100 mM DTT. Template DNA was removed by the addition of 2 μl of RQ DNase (1 U ml^{-1}) (Promega). Unincorporated nucleotides were removed by G50 spin columns (GE Healthcare) according to the manufacturer's instructions, in a final volume of 30 μl. For *E. coli* tRNA^{Trp}, the transcript reaction was gel-purified on a denaturing 5% acrylamide gel and eluted in 0.3 M sodium acetate for 4 hours overnight at 4°C. The supernatant was removed, ethanol-precipitated, and resuspended in 20 to 30 μl of nuclease-free H_2O.

Nucleotide transfer assays

MenT$_3$ NTase activity was assayed in 10-μl reaction volumes containing 50 mM tris-HCl (pH 9.5), 10 mM $MgCl_2$, and 2.5 mM rNTPs and incubated for 20 min at 37°C. Fresh, uniformly labeled tRNA (0.5 μl) was used per assay, with different dilutions of the protein (1, 0.1, 0.01, and 0.001 mg ml^{-1}) in 50 mM tris-HCl (pH 7.8), 300 mM NaCl, and 10% glycerol. The 10-μl reactions were mixed directly with 10 μl of RNA loading dye (95% formamide, 1 mM EDTA, 0.025% SDS, xylene cyanol, and bromophenol blue), denatured at 90°C, and applied to 5% polyacrylamide-urea gels. The gel was vacuum-dried at 80°C and exposed to a PhosphorImager screen.

In vitro antitoxicity assays

The effect of MenA$_3$ antitoxin was assayed using in vitro-transcribed tRNA^{Ser2} as a substrate. For the coincubation assay, MenT$_3$ (5 μM) and increasing molar ratios of MenA$_3$ were incubated with tRNA^{Ser2} and 2.5 mM CTP in 10-μl reaction volumes containing 50 mM tris-HCl (pH 9.5) and 10 mM $MgCl_2$ for 20 min at 37°C. For the postincubation assay, the reactions were first incubated for 20 min at 37°C with MenT$_3$ alone in 7-μl reaction volumes, then 3 μl containing different concentrations of MenA$_3$ were added, and the reactions were incubated for a further 20 min at 37°C.

MenT$_3$ tRNA screening

The tRNA screening was performed using 0.5 μl of uniformly labeled *M. tuberculosis* tRNAs, all containing the CCA motif. The activity

was tested in 50 mM tris-HCl (pH 9.5), 10 mM $MgCl_2$, and 2.5 mM rCTP in 10-μl reaction volumes and incubated for 20 min at 37°C. The transcripts were incubated with 1 μl of $MenT_3$ (0.1 mg ml^{-1}), or with nuclease-free water as a control. The reaction was stopped with 10 μl of RNA loading dye (95% formamide, 1 mM EDTA, 0.025% SDS, xylene cyanol, and bromophenol blue), denatured at 90°C, and applied to 5% polyacrylamide-urea gels. The gel was vacuum-dried at 80°C and exposed to a PhosphorImager screen.

SUPPLEMENTARY MATERIALS

Supplementary material for this article is available at http://advances.sciencemag.org/cgi/content/full/6/31/eabb6651/DC1

View/request a protocol for this paper from *Bio-protocol*.

REFERENCES AND NOTES

1. J. P. Norton, M. A. Mulvey, Toxin-antitoxin systems are important for niche-specific colonization and stress resistance of uropathogenic *Escherichia coli*. *PLOS Pathog.* **8**, e1002954 (2012).
2. S. Helaine, A. M. Cheverton, K. G. Watson, L. M. Faure, S. A. Matthews, D. W. Holden, Internalization of *Salmonella* by macrophages induces formation of nonreplicating persisters. *Science* **343**, 204–208 (2014).
3. R. Page, W. Peti, Toxin-antitoxin systems in bacterial growth arrest and persistence. *Nat. Chem. Biol.* **12**, 208–214 (2016).
4. P. C. Fineran, T. R. Blower, I. J. Foulds, D. P. Humphreys, K. S. Lilley, G. P. Salmond, The phage abortive infection system, ToxIN, functions as a protein-RNA toxin-antitoxin pair. *Proc. Natl. Acad. Sci. U.S.A.* **106**, 894–899 (2009).
5. D. C. Pecota, T. K. Wood, Exclusion of T4 phage by the *hok/sok* killer locus from plasmid R1. *J. Bacteriol.* **178**, 2044–2050 (1996).
6. F. Goormaghtigh, N. Fraikin, M. Putrinš, T. Hallaert, V. Hauryliuk, A. Garcia-Pino, A. Sjödin, S. Kasvandik, K. Udekwu, T. Tenson, N. Kaldalu, L. Van Melderen, Reassessing the role of Type II toxin-antitoxin systems in formation of *Escherichia coli* Type II persister cells. *MBio* **9**, e00640–18 (2018).
7. M. H. Pontes, E. A. Groisman, Slow growth determines nonheritable antibiotic resistance in *Salmonella enterica*. *Sci. Signal.* **12**, eaax3938 (2019).
8. M. LeRoux, P. H. Culviner, Y. J. Liu, M. L. Littlehale, M. T. Laub, Stress induces the transcription of toxin-antitoxin systems but does not activate the toxin. *bioRxiv*, (2020).
9. S. Ronneau, S. Helaine, Clarifying the link between toxin–antitoxin modules and bacterial persistence. *J. Mol. Biol.* **431**, 3462–3471 (2019).
10. N. Fraikin, F. Goormaghtigh, L. Van Melderen, Type II toxin-antitoxin systems: Evolution and revolutions. *J. Bacteriol.* **202**, e00763-19 (2020).
11. S. Szekeres, M. Dauti, C. Wilde, D. Mazel, D. A. Rowe-Magnus, Chromosomal toxin-antitoxin loci can diminish large-scale genome reductions in the absence of selection. *Mol. Microbiol.* **63**, 1588–1605 (2007).
12. S. Song, T. K. Wood, Toxin/antitoxin system paradigms: Toxins bound to antitoxins are not likely activated by preferential antitoxin degradation. *Adv. Biosyst.* **4**, 1900290 (2020).
13. A. M. Hall, B. Gollan, S. Helaine, Toxin–antitoxin systems: Reversible toxicity. *Curr. Opin. Microbiol.* **36**, 102–110 (2017).
14. I. Keren, S. Minami, E. Rubin, K. Lewis, Characterization and transcriptome analysis of *Mycobacterium tuberculosis* persisters. *MBio* **2**, e00100–11 (2011).
15. A. Sala, P. Bordes, P. Genevaux, Multiple toxin-antitoxin systems in *Mycobacterium tuberculosis*. *Toxins* **6**, 1002–1020 (2014).
16. H. Akarsu, P. Bordes, M. Mansour, D.-J. Bigot, P. Genevaux, L. Falquet, TASmania: A bacterial Toxin-Antitoxin Systems database. *PLoS Comput. Biol.* **15**, e1006946 (2019).
17. H. R. Ramage, L. E. Connolly, J. S. Cox, Comprehensive functional analysis of *Mycobacterium tuberculosis* toxin-antitoxin systems: Implications for pathogenesis, stress responses, and evolution. *PLOS Genet.* **5**, e1000767 (2009).
18. D. M. Freire, C. Gutierrez, A. Garza-Garcia, A. D. Grabowska, A. J. Sala, K. Ariyachaokun, T. Panikova, K. S. H. Beckham, A. Colom, V. Pogenberg, M. Cianci, A. Tuukkanen, Y.-M. Boudehen, A. Peixoto, L. Botella, D. I. Svergun, D. Schnappinger, T. R. Schneider, P. Genevaux, L. P. S. de Carvalho, M. Wilmanns, A. H. A. Parret, O. Neyrolles, An NAD+ phosphorylase toxin triggers *Mycobacterium tuberculosis* cell death. *Mol. Cell* **73**, 1282–1291.e8 (2019).
19. P. Garvey, G. F. Fitzgerald, C. Hill, Cloning and DNA sequence analysis of two abortive infection phage resistance determinants from the lactococcal plasmid pNP40. *Appl. Environ. Microbiol.* **61**, 4321–4328 (1995).
20. R. L. Dy, R. Przybilski, K. Semeijn, G. P. C. Salmond, P. C. Fineran, A widespread bacteriophage abortive infection system functions through a Type IV toxin-antitoxin mechanism. *Nucleic Acids Res.* **42**, 4590–4605 (2014).
21. F. Li, Y. Xiong, J. Wang, H. D. Cho, K. Tomita, A. M. Weiner, T. A. Steitz, Crystal structures of the *Bacillus stearothermophilus* CCA-adding enzyme and its complexes with ATP or CTP. *Cell* **111**, 815–824 (2002).
22. H. G. Hampton, S. A. Jackson, R. D. Fagerlund, A. I. M. Vogel, R. L. Dy, T. R. Blower, P. C. Fineran, AbiEi binds cooperatively to the Type IV abiE toxin–antitoxin operator via a positively-charged surface and causes DNA bending and negative autoregulation. *J. Mol. Biol.* **430**, 1141–1156 (2018).
23. C. M. Sassetti, D. H. Boyd, E. J. Rubin, Genes required for mycobacterial growth defined by high density mutagenesis. *Mol. Microbiol.* **48**, 77–84 (2003).
24. M. A. Dejesus, E. R. Gerrick, W. Xu, S. W. Park, J. E. Long, C. C. Boutte, E. J. Rubin, D. Schnappinger, S. Ehrt, S. M. Fortune, C. M. Sassetti, T. R. Ioerger, Comprehensive essentiality analysis of the *Mycobacterium tuberculosis* genome via saturating transposon mutagenesis. *MBio* **8**, e02133–16 (2017).
25. L. Holm, C. Sander, Protein structure comparison by alignment of distance matrices. *J. Mol. Biol.* **233**, 123–138 (1993).
26. Y. Zhao, X. Ye, Y. Su, L. Sun, F. She, Y. Wu, Crystal structure confirmation of JHP933 as a nucleotidyltransferase superfamily protein from *Helicobacter pylori* strain J99. *PLOS ONE* **9**, e104609 (2014).
27. S. Bost, F. Silva, D. Belin, Transcriptional activation of *ydeA*, which encodes a member of the major facilitator superfamily, interferes with arabinose accumulation and induction of the *Escherichia coli* arabinose P_{BAD} promoter. *J. Bacteriol.* **181**, 2185–2191 (1999).
28. D. H. Bechhofer, M. P. Deutscher, Bacterial ribonucleases and their roles in RNA metabolism. *Crit. Rev. Biochem. Mol. Biol.* **54**, 242–300 (2019).
29. B. D. Janssen, E. J. Diner, C. S. Hayes, in *Bacterial Regulatory RNA* (Humana Press, 2012; www.ncbi.nlm.nih.gov/pubmed/22736012), vol. 905, pp. 291–309.
30. P. P. Chan, T. M. Lowe, GtRNAdb 2.0: An expanded database of transfer RNA genes identified in complete and draft genomes. *Nucleic Acids Res.* **44**, D184–D189 (2016).
31. L. Samhita, V. Nanjundiah, U. Varshney, How many initiator tRNA genes does *Escherichia coli* need? *J. Bacteriol.* **196**, 2607–2615 (2014).
32. B. Lenhard, O. Orellana, M. Ibba, I. Weygand-Durasević, tRNA recognition and evolution of determinants in seryl-tRNA synthesis. *Nucleic Acids Res.* **27**, 721–729 (1999).
33. G. Jankevicius, A. Ariza, M. Ahel, I. Ahel, The toxin-antitoxin system DarTG catalyzes reversible ADP-ribosylation of DNA. *Mol. Cell* **64**, 1109–1116 (2016).
34. K. S. Winther, D. E. Brodersen, A. K. Brown, K. Gerdes, VapC20 of *Mycobacterium tuberculosis* cleaves the Sarcin–Ricin loop of 23S rRNA. *Nat. Commun.* **4**, 2796 (2013).
35. A. M. Cheverton, B. Gollan, M. Przydacz, C. T. Wong, A. Mylona, S. A. Hare, S. Helaine, A *Salmonella* toxin promotes persister formation through acetylation of tRNA. *Mol. Cell* **63**, 86–96 (2016).
36. D. Jurėnas, S. Chatterjee, A. Konijnenberg, F. Sobott, L. Droogmans, A. Garcia-Pino, L. Van Melderen, AtaT blocks translation initiation by N-acetylation of the initiator $tRNA^{fMet}$. *Nat. Chem. Biol.* **13**, 640–646 (2017).
37. J.-Y. Bouet, M. Bouvier, D. Lane, Concerted action of plasmid maintenance functions: Partition complexes create a requirement for dimer resolution. *Mol. Microbiol.* **62**, 1447–1459 (2006).
38. K. A. Datsenko, B. L. Wanner, One-step inactivation of chromosomal genes in *Escherichia coli* K-12 using PCR products. *Proc. Natl. Acad. Sci. U.S.A.* **97**, 6640–6645 (2000).
39. M. P. Mayer, A new set of useful cloning and expression vectors derived from pBlueScript. *Gene* **163**, 41–46 (1995).
40. P. Genevaux, F. Keppel, F. Schwager, P. S. Langendijk-Genevaux, F. U. Hartl, C. Georgopoulos, *In vivo* analysis of the overlapping functions of DnaK and trigger factor. *EMBO Rep.* **5**, 195–200 (2004).
41. A. Blumenthal, C. Trujillo, S. Ehrt, D. Schnappinger, Simultaneous analysis of multiple *Mycobacterium tuberculosis* knockdown mutants *in vitro* and *in vivo*. *PLOS ONE* **5**, e15667 (2010).
42. L. Botella, J. Vaubourgeix, J. Livny, D. Schnappinger, Depleting *Mycobacterium tuberculosis* of the transcription termination factor Rho causes pervasive transcription and rapid death. *Nat. Commun.* **8**, 14731 (2017).
43. J. C. van Kessel, G. F. Hatfull, Recombineering in *Mycobacterium tuberculosis*. *Nat. Methods* **4**, 147–152 (2007).
44. L. M. Guzman, D. Belin, M. J. Carson, J. Beckwith, Tight regulation, modulation, and high-level expression by vectors containing the arabinose P_{BAD} promoter. *J. Bacteriol.* **177**, 4121–4130 (1995).
45. J. Peränen, M. Rikkonen, M. Hyvönen, L. Kääriäinen, T7 vectors with a modified T7*lac* promoter for expression of proteins in *Escherichia coli*. *Anal. Biochem.* **236**, 371–373 (1996).
46. S. Ehrt, X. V. Guo, C. M. Hickey, M. Ryou, M. Monteleone, L. W. Riley, D. Schnappinger, Controlling gene expression in mycobacteria with anhydrotetracycline and Tet repressor. *Nucleic Acids Res.* **33**, e21 (2005).
47. Y.-M. Boudehen, M. Wallat, P. Rousseau, O. Neyrolles, C. Gutierrez, An improved Xer-cise technology for the generation of multiple unmarked mutants in mycobacteria. *Biotechniques* **68**, 106–110 (2020).

48. F. Anglès, M.-P. Castanié-Cornet, N. Slama, M. Dinclaux, A.-M. Cirinesi, J.-C. Portais, F. Létisse, P. Genevaux, Multilevel interaction of the DnaK/DnaJ(HSP70/HSP40) stress-responsive chaperone machine with the central metabolism. *Sci. Rep.* **7**, 41341 (2017).
49. W. Kabsch, XDS. *Acta Crystallogr. D Biol. Crystallogr.* **66**, 125–132 (2010).
50. M. D. Winn, C. C. Ballard, K. D. Cowtan, E. J. Dodson, P. Emsley, P. R. Evans, R. M. Keegan, E. B. Krissinel, A. G. W. Leslie, A. McCoy, S. J. McNicholas, G. N. Murshudov, N. S. Pannu, E. A. Potterton, H. R. Powell, R. J. Read, A. Vagin, K. S. Wilson, Overview of the CCP4 suite and current developments. *Acta Crystallogr. D Biol. Crystallogr.* **67**, 235–242 (2011).
51. D. D. Rodríguez, C. Grosse, S. Himmel, C. González, I. M. de Ilarduya, S. Becker, G. M. Sheldrick, I. Usón, Crystallographic *ab initio* protein structure solution below atomic resolution. *Nat. Methods* **6**, 651–653 (2009).
52. P. D. Adams, P. V. Afonine, G. Bunkóczi, V. B. Chen, I. W. Davis, N. Echols, J. J. Headd, L.-W. Hung, G. J. Kapral, R. W. Grosse-Kunstleve, A. J. McCoy, N. W. Moriarty, R. Oeffner, R. J. Read, D. C. Richardson, J. S. Richardson, T. C. Terwilliger, P. H. Zwart, PHENIX: A comprehensive Python-based system for macromolecular structure solution. *Acta Crystallogr. D Biol. Crystallogr.* **66**, 213–221 (2010).
53. P. Emsley, K. Cowtan, Coot: Model-building tools for molecular graphics. *Acta Crystallogr. D Biol. Crystallogr.* **60**, 2126–2132 (2004).
54. P. Bordes, A. J. Sala, S. Ayala, P. Texier, N. Slama, A. M. Cirinesi, V. Guillet, L. Mourey, P. Genevaux, Chaperone addiction of toxin-antitoxin systems. *Nat. Commun.* **7**, 13339 (2016).
55. T. S. Stenum, M. A. Sørensen, S. Lo Svenningsen, Quantification of the abundance and charging levels of transfer RNAs in *Escherichia coli*. *J. Vis. Exp.* **22**, 56212 (2017).
56. V. Khemici, J. Prados, P. Linder, P. Redder, Decay-initiating endoribonucleolytic cleavage by RNase Y is kept under tight control via sequence preference and sub-cellular localisation. *PLOS Genet.* **11**, e1005577 (2015).

Acknowledgments: We thank D.-J. Bigot for plasmid constructs, and P. Bordes, M.-P. Castanié-Cornet, L. Falquet, L. Poljak, L. Hadjeras, and H. Akarsu for valuable advice. We also thank K. Semeijn and R. Dy for initial plasmid construction and testing, and E. Naser (Genotoul TRI-IPBS imaging facility) for help with flow cytometry analysis. **Funding:** This work was supported by a scholarship from the China Scholarship Council (CSC) as part of a joint international PhD program with Toulouse University Paul Sabatier (Y.C.); Springboard Award (SBF002\1104) from the Academy of Medical Sciences (B.U. and T.R.B.); University of Otago Research Grant (P.C.F.), the School of Biomedical Sciences Bequest Fund, and University of Otago (P.C.F.); CNRS (UPR 9073), Université Paris VII-Denis Diderot, the Agence Nationale de la Recherche (ARNr-QC), and the Labex (Dynamo) program (A.T. and C.C.); European Commission (contracts NEWTBVAC n°241745 and TBVAC2020 n°643381), Centre National de la Recherche Scientifique, Université Paul Sabatier, Agence Nationale de la Recherche (ANR-13-BSV8-0010-01), and Fondation pour la Recherche Médicale (DEQ20160334902) (C.G. and O.N.); and grant SNF CRSII3_160703 (P.G.).
Author contributions: Conceptualization, all authors. Investigation, Y.C., B.U., C.G., A.T., and M. M. Writing, all authors. Funding acquisition, P.C.F., C.C., O.N., P.G., and T.R.B. Supervision, C.C., O.N., P.G., and T.R.B. **Competing interests:** The authors declare that they have no competing interests. **Data and materials availability:** The crystal structures of $MenT_3$ and $MenT_4$ have been deposited in the Protein Data Bank under accession numbers 6Y5U and 6Y56, respectively. All data needed to evaluate the conclusions in the paper are present in the paper and/or the Supplementary Materials. Additional data related to this paper may be requested from the authors.

Submitted 10 March 2020
Accepted 12 June 2020
Published 29 July 2020
10.1126/sciadv.abb6651

Citation: Y. Cai, B. Usher, C. Gutierrez, A. Tolcan, M. Mansour, P. C. Fineran, C. Condon, O. Neyrolles, P. Genevaux, T. R. Blower, A nucleotidyltransferase toxin inhibits growth of *Mycobacterium tuberculosis* through inactivation of tRNA acceptor stems. *Sci. Adv.* **6**, eabb6651 (2020).

Science Advances

A nucleotidyltransferase toxin inhibits growth of *Mycobacterium tuberculosis* through inactivation of tRNA acceptor stems

Yiming Cai, Ben Usher, Claude Gutierrez, Anastasia Tolcan, Moise Mansour, Peter C. Fineran, Ciarán Condon, Olivier Neyrolles, Pierre Genevaux and Tim R. Blower

Sci Adv **6** (31), eabb6651.
DOI: 10.1126/sciadv.abb6651